

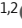



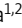




ARTICLE

PKM2 promotes Th17 cell differentiation and autoimmune inflammation by fine-tuning STAT3 activation

Luis Eduardo Alves Damasceno^{1,2} , Douglas Silva Prado^{1,2} , Flavio Protasio Veras^{1,2}, Miriam M. Fonseca^{1,2} , Juliana E. Toller-Kawahisa^{1,2}, Marcos Henrique Rosa^{1,2} , Gabriel Azevedo Públio^{1,2} , Timna Varela Martins^{1,2}, Fernando S. Ramalho³, Ari Waisman⁴ , Fernando Queiroz Cunha^{1,2} , Thiago Mattar Cunha^{1,2} , and José Carlos Alves-Filho^{1,2} 

Th17 cell differentiation and pathogenicity depend on metabolic reprogramming inducing shifts toward glycolysis. Here, we show that the pyruvate kinase M2 (PKM2), a glycolytic enzyme required for cancer cell proliferation and tumor progression, is a key factor mediating Th17 cell differentiation and autoimmune inflammation. We found that PKM2 is highly expressed throughout the differentiation of Th17 cells in vitro and during experimental autoimmune encephalomyelitis (EAE) development. Strikingly, PKM2 is not required for the metabolic reprogramming and proliferative capacity of Th17 cells. However, T cell-specific PKM2 deletion impairs Th17 cell differentiation and ameliorates symptoms of EAE by decreasing Th17 cell-mediated inflammation and demyelination. Mechanistically, PKM2 translocates into the nucleus and interacts with STAT3, enhancing its activation and thereby increasing Th17 cell differentiation. Thus, PKM2 acts as a critical nonmetabolic regulator that fine-tunes Th17 cell differentiation and function in autoimmune-mediated inflammation.

Introduction

Th17 cells are critical components of the adaptive immunity that contribute to the host defense against extracellular pathogens, but they are also implicated in the pathogenesis of autoimmune-mediated inflammatory diseases (Korn et al., 2009). Cosignaling of IL-6 and TGF- β induces the differentiation of Th17 cells (Veldhoen et al., 2006; Bettelli et al., 2006; Mangan et al., 2006). IL-6 drives the phosphorylation of STAT3 that translocates into the nucleus and induces the expression of the transcription factors Ror α and Ror γ t (Ivanov et al., 2006; Yang et al., 2007, 2008). TGF- β inhibits IL-6-induced SOCS3 expression, thus prolonging STAT3 activation (Qin et al., 2009; Chen et al., 2006). In combination with other transcription factors, STAT3 and retinoic acid orphan receptor gamma T synergize to regulate transcription of the T helper type 17 (Th17) cell-signature genes IL-17A, IL-17F, IL-22, and IL-23R (Korn et al., 2009). Another cytokine, IL-23, mediates the final differentiation, stabilization, and induction of GM-CSF production by Th17 cells, making these cells pathogenic (El-Behi et al., 2011; Codarri et al., 2011; McGeachy et al., 2009). However, much remains unclear about

the regulatory signaling pathways that control the differentiation and pathogenicity of Th17 cells.

Recent studies have shown that immune cells undergo a dynamic metabolic reprogramming to support the bioenergetic and biosynthetic requirements for proper activation, proliferation, and differentiation. Mammalian target of rapamycin complex 1 (mTORC1) and hypoxia-inducible factor 1 α (HIF1 α) are critical regulators of cellular metabolism and also have a central role in controlling immune cell activation and functions (O'Neill et al., 2016; Buck et al., 2015; Almeida et al., 2016). Indeed, the HIF1 α - and mTORC1-dependent metabolic reprogramming toward aerobic glycolysis, a phenomenon that resembles the well-described Warburg effect in tumor cells, is also especially important for Th17 cell development (Shi et al., 2011; Delgoffe et al., 2011; Dang et al., 2011; Kurebayashi et al., 2012). Consistent with this, the blockade of glycolysis with 2-deoxyglucose inhibits Th17 cell generation in vitro and ameliorates the development of experimental autoimmune encephalomyelitis (EAE; Shi et al., 2011).

¹Department of Pharmacology, Ribeirao Preto Medical School, University of Sao Paulo, Ribeirao Preto, Brazil; ²Center for Research in Inflammatory Diseases, Ribeirao Preto Medical School, University of Sao Paulo, Ribeirao Preto, Brazil; ³Department of Pathology, Ribeirao Preto Medical School, University of Sao Paulo, Ribeirao Preto, Brazil; ⁴Institute for Molecular Medicine, University Medical Center of the Johannes Gutenberg-University, Mainz, Germany.

Correspondence to Jose C. Alves-Filho: jcafilho@usp.br.

© 2020 Damasceno et al. This article is distributed under the terms of an Attribution-Noncommercial-Share Alike-No Mirror Sites license for the first six months after the publication date (see <http://www.rupress.org/terms/>). After six months it is available under a Creative Commons License (Attribution-Noncommercial-Share Alike 4.0 International license, as described at <https://creativecommons.org/licenses/by-nc-sa/4.0/>).

Pyruvate kinase (PK) is a glycolytic enzyme that converts phosphoenolpyruvate to pyruvate (Israelsen and Vander Heiden, 2015; Gui et al., 2013). Four isoforms of PK are present in mammals and differentially distributed according to the cell type. Particularly, expressions of the PK isoforms M1 (PKM1) and M2 (PKM2) are derived through alternative splicing of the *Pkm* gene (Noguchi et al., 1986). PKM1 is constitutively expressed at a constant level in most tissues, while PKM2 is mainly expressed in proliferating and tumor cells. Structurally, PKM1 forms constitutive and stable tetramers with high metabolic activity, whereas the PKM2 tetrameric conformation requires allosteric modulation, being mostly expressed as metabolically inactive monomeric and dimeric forms (Israelsen and Vander Heiden, 2015; Gui et al., 2013). Although the dimeric PKM2 has low metabolic activity, it gains the ability to translocate into the nucleus and act as a nuclear transcriptional coactivator, regulating gene expression by interaction with some transcriptional factors, including HIF1 α (Yang et al., 2011; Luo et al., 2011; Yang et al., 2012a). Pharmacological inhibition of PKM2 nuclear translocation or its silencing decreases aerobic glycolysis and the proliferation of tumor cells (Christofk et al., 2008; Anastasiou et al., 2012). Moreover, recent reports show that PKM2 regulates the production of inflammatory cytokines in LPS-activated macrophages (Shirai et al., 2016; Yang et al., 2014; Palsson-McDermott et al., 2015).

In this study, we demonstrated that PKM2 mediates the differentiation of Th17 cells, but not Th1, Th2, or regulatory T (T_{reg}) cells, through activation of STAT3. We found that the dimeric PKM2 translocates into the nucleus and interacts with STAT3, enhancing its phosphorylated status throughout the differentiation of Th17 cells. T cell-specific PKM2 deletion impairs the development of Th17 cells and ameliorates symptoms of EAE by decreasing Th17 cell-mediated inflammation and demyelination. PKM2 therefore represents a potential therapeutic target for autoimmune-mediated inflammation.

Results

Th17 cells express PKM2 throughout differentiation

To determine the role of PKM2 in the activation, proliferation, and differentiation of T cells, we initially analyzed the expression of PKM splice isoforms in Th cell subtypes. To this end, we cultured naive CD4⁺CD25⁻ T cells from C57BL/6 mice under Th1, Th2, Th17, and induced T_{reg} (iT_{reg}) cell-polarizing conditions in vitro to obtain T cells with selective expression of *Ifng*, *Il4*, *Il17a*, and *Foxp3*, respectively (Fig. S1 A). As controls, naive CD4⁺CD25⁻ T cells were activated with anti-CD3 ϵ /CD28 antibodies without the addition of differentiating cytokines (Th0 cells). We found that *Pkm1* mRNA is constitutively expressed in freshly isolated naive T cells and did not increase substantially in Th cell subtypes, whereas *Pkm2* mRNA expression was up-regulated in all Th cell subtypes when compared with naive T cells at 48 h of culture. However, significantly more *Pkm2* mRNA expression was observed in Th17 cells (Fig. 1 A). Of note, effector/memory CD62L^{lo}CD44^{hi} CD4⁺ T cells in homeostatic conditions show a slight increase in *Pkm2* mRNA expression, but not *Pkm1*, in comparison to naive cells, but lower than that observed in fully differentiated Th17 cells in vitro (Fig. S1 B).

In a kinetic analysis of Th17 cell differentiation, *Pkm2* mRNA expression was detectable at 24 h, and it reached a peak at 48 h of culture, whereas *Pkm1* expression remained constant throughout differentiation (Fig. 1 B). Immunoblot analysis confirmed that PKM2 protein levels were very low or undetectable in naive T cells. However, it markedly increased throughout Th17 cell differentiation, while PKM1 protein expression is constitutively expressed in resting naive T cells showing a slight increase in differentiated Th17 cells (Fig. 1 C). According to our findings on *Pkm2* gene expression, PKM2 protein expression was higher in Th17 cells than Th1 cells (Fig. S1 C). Additionally, using the flow cytometry approach, we observed that IL-17A⁺ CD4⁺ T cells exhibited higher intracellular staining for PKM2 than IL-17A⁻ CD4⁺ T cells from the same culture wells after Th17 differentiation. Moreover, the addition of IL-23 to the cell cultures concomitantly increased both Th17 cell differentiation and PKM2 expression in IL-17A-producing T cells (Fig. 1 D).

mTORC1 signaling up-regulates the expression of PKM2 in tumor cells (Sun et al., 2011), whereas T cell-specific deletion of mTORC1 activity impairs Th17 differentiation in vitro and in vivo (Kurebayashi et al., 2012; Delgoffe et al., 2011). We therefore investigated whether mTORC1 signaling is involved in the expression of PKM2 during the differentiation of Th17 cells. As expected, inhibition of mTOR with rapamycin dramatically reduced IL-17A and increased Foxp3 expression in CD4⁺ T cells cultured under Th17 cell-polarizing conditions (Fig. S1, D and E). Rapamycin did not affect *Pkm1* expression, but it significantly reduced PKM2 mRNA and protein expression (Fig. 1, E and F).

These observations led us to determine if the expression of PKM2 changes in a Th17 cell-mediated inflammatory disease model (Sie et al., 2014). Its expression profile was evaluated throughout the course of EAE development. This was done by immunizing mice with myelin oligodendrocyte glycoprotein (MOG)_{35–55} peptide (Fig. 2, A and B). We found that *Pkm2* mRNA expression had increased in draining LNs (DLNs) before disease onset (day 10) and in the spinal cord at the peak of the EAE symptoms (day 15) following the expression profile observed with the transcription of Th17 cell-related genes, such as *Il17a*, *Csf2*, and *Il23r* (Fig. 2 C). Immunoblot analysis confirmed the increased PKM2 protein levels in the spinal cord of EAE mice (Fig. 2 D). Moreover, histopathological analysis with H&E and immunofluorescent staining of spinal cord lesions in EAE mice showed that PKM2 expression was confined almost exclusively into the inflammatory cell infiltration region, while absent in spinal cord sections of naive mice (Fig. 2 E). Consistent with this, CD4⁺ T cells isolated from the spinal cords of EAE mice expressed significantly higher *Pkm2* mRNA transcription levels along with the Th17 cell-related genes *Il17a*, *Csf2*, *Il23r*, *Rora*, and *Rorc* compared with CD45⁺ cells from the spinal cord of naive mice (Fig. 2 F). Taken together, these results indicate that PKM2 expression is induced in Th17 cells in vitro and in vivo, suggesting that it might affect their differentiation.

Th17 cells require PKM2 for the complete differentiation

Activated T cells undergo a dynamic metabolic reprogramming to support the bioenergetic and biosynthetic demands for proper proliferation and differentiation (Buck et al., 2015; Almeida

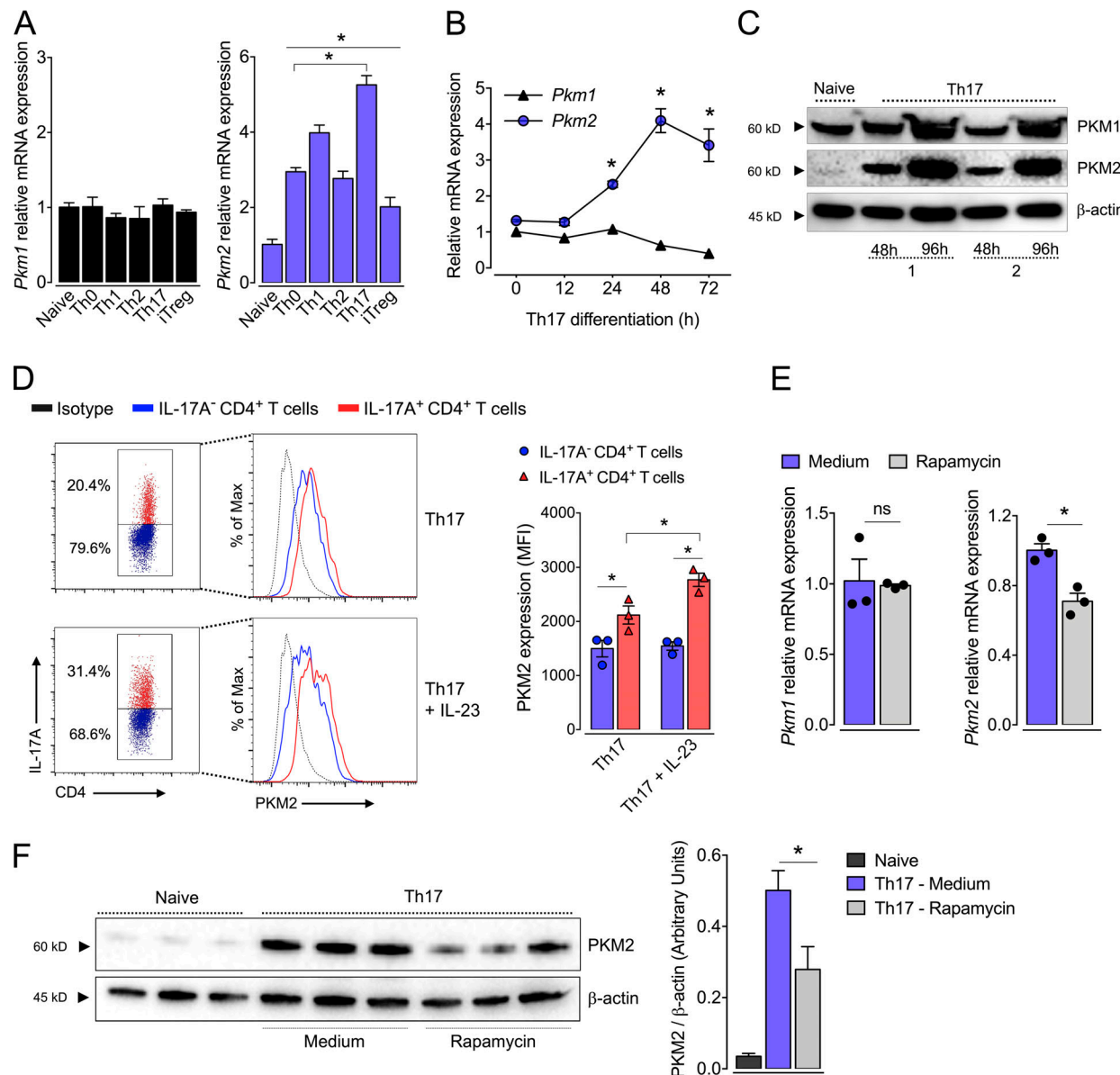


Figure 1. Th17 cell differentiation accompanies high PKM2 expression levels. (A) *Pkm1* and *Pkm2* gene expression were evaluated by RT-qPCR in freshly isolated CD4 T cells (naive) and polyclonally activated CD4 T cells (Th0) and Th1, Th2, Th17, and iT reg cells at 48 h after culture ($n = 3$). (B) Naive CD4 T cells were differentiated into Th17 cells, and gene expression of *Pkm1* and *Pkm2* was determined at different time points by RT-qPCR ($n = 3$). (C) Protein expression levels of PKM1 and PKM2 during Th17 cell differentiation were detected by immunoblot; β-actin was used as a loading control. (D) Th17 cells were differentiated in the presence or absence of IL-23, and PKM2 expression was determined by flow cytometry. MFI, mean fluorescence intensity. (E) Rapamycin (0.1 μM), an mTOR inhibitor, was added to the Th17 cell cultures. After 96 h, cells were collected, and the expression of *Pkm1* and *Pkm2* was determined by RT-qPCR. For gene expression analysis, the cycle threshold values were normalized to *Gapdh*; fold change was calculated relative to untreated cells ($n = 3$). (F) Rapamycin-treated Th17 cells were also collected for immunoblot analysis of PKM2 protein levels ($n = 3$). β-Actin was used as a loading control. Data are representative of two independent experiments. Error bars show mean ± SEM. P values were determined by one-way ANOVA followed by Tukey's post hoc test (A and F), two-way ANOVA followed by Tukey's post hoc test (B and D), or two-tailed Student's *t* test (E). *, $P < 0.05$; ns, not significant.

et al., 2016). Cancer cells and macrophages require PKM2 expression for their metabolic reprogramming toward aerobic glycolysis (Palsson-McDermott et al., 2015; Christofk et al., 2008), whereas defective glycolysis dramatically impairs Th17 cell differentiation and proliferation (Shi et al., 2011). We hypothesized that similar to macrophages and tumor cells, PKM2 up-regulation would also be required for metabolic reprogramming of T cells. To test this hypothesis, we crossed mice carrying

the LoxP-flanked *Pkm2*-specific exon 10 (*Pkm2*^{fl/fl}; Israelsen et al., 2013) with CD4^{Cre} mice (Lee et al., 2001) to generate T cell-specific PKM2 deficient mice (CD4^{Cre}*Pkm2*^{fl/fl}). Littermates *Pkm2*^{fl/fl} and CD4^{Cre} mice were used as WT controls. No significant difference in LN and spleen sizes were observed between WT or CD4^{Cre}*Pkm2*^{fl/fl} mice (Fig. S2 A), and CD4^{Cre}*Pkm2*^{fl/fl} pups did not display any apparent abnormalities, presenting a grossly healthy development (data not shown).

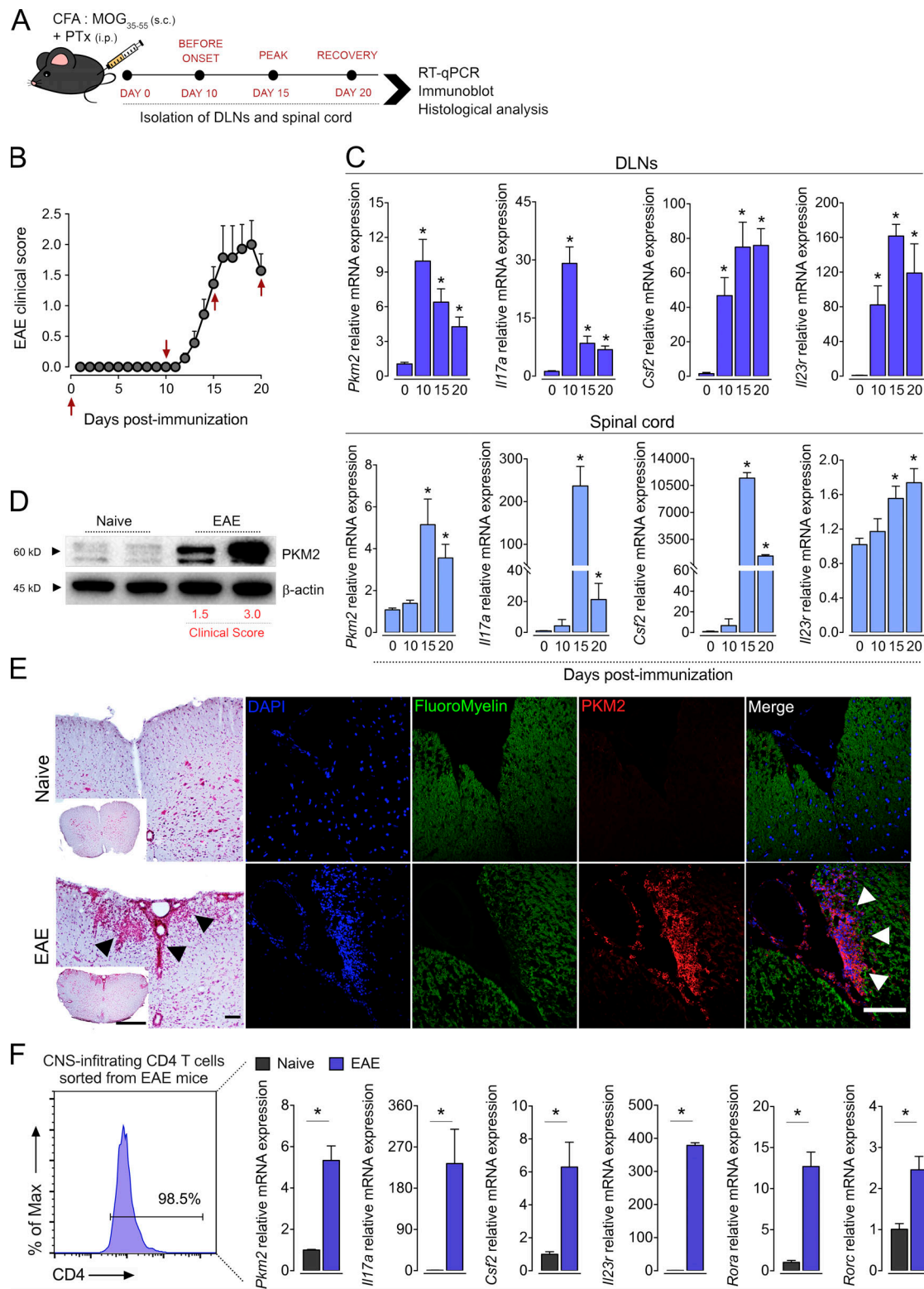


Figure 2. PKM2 expression increases during EAE development. (A and B) EAE was induced in WT C57BL/6 mice by subcutaneous immunization with MOG₃₅₋₅₅; the clinical score was evaluated throughout the days after immunization. (C) DLNs (top) and spinal cord samples (bottom) were collected at the indicated time points depicted in B (red arrows) for analysis of *Pkm2*, *Il17a*, *Csf2*, and *Il23r* gene expression by RT-qPCR ($n = 7$ per time point). Cycle threshold values were normalized to *Gapdh*. (D) PKM2 total protein levels in the spinal cord of EAE-bearing mice were determined by immunoblot; β -actin was used as a loading control. (E) Inflammatory cell infiltration was observed in the spinal cord by using H&E staining (left; black arrows). Scale bar indicates 500 and 50 μ m. PKM2 protein expression in the spinal cord was analyzed by immunofluorescence (red); DAPI was used as a nuclear marker (blue), and myelin was stained with fluoromyelin stain probe (green; $n = 3$). Scale bar represents 50 μ m. (F) Mononuclear cells were isolated from CNS of naive and EAE mice ($n = 9$ per group) followed by magnetic separation of CD4 T cells. Expression of *Pkm2*, *Il17a*, *Csf2*, *Il23r*, *Rora*, and *Rorc* was analyzed by RT-qPCR. Each sample was a pool of three

mice. Cycle threshold values were normalized to *Gapdh*, and fold change was calculated relative to CNS CD45⁺ cells from naive mice. Data are representative of two (C, E, and F) or three (D) independent experiments. Error bars indicate mean \pm SEM. P values were determined by two-tailed Student's *t* test (C and F). *, *P* < 0.05.

Moreover, the proportion of CD4 or CD8 T cells in the thymus and the frequency of naive or memory CD4 T cell populations in LNs and spleen was not significantly different between WT and CD4^{Cre}*Pkm2*^{fl/fl} mice (Fig. S2, B–D).

We then cultured naive PKM2-deficient CD4 T cells under a Th17 cell-polarizing condition and examined the expression levels of key molecules required for glycolysis (Fig. 3A). The loss of *Pkm2* in CD4 T cells was confirmed by immunoblot analysis of PKM2 protein expression in Th17 cells after 72 h in culture (Fig. 3B). Consistent with previous studies, WT Th17 cells showed increased expression of *Slc2a1* (the gene encoding glucose transporter GLUT1), *Ldha* (lactate dehydrogenase [LDH]), and *Hif1a* (HIF1 α) compared with naive CD4 T cells (Fig. 3C). Strikingly, PKM2 deficiency did not affect the expression of

those proglycolytic genes (Fig. 3C). Correspondingly, LDH and HIF1 α proteins levels were also comparable between WT and PKM2-deficient Th17 cells (Fig. 3D). Nevertheless, deficiency of PKM2 led to compensatory up-regulation of PKM1 expression (Fig. 3, B and C). Thus, we next examined whether PKM2 affects the glucose metabolism of Th17 cells. This evaluation was performed by monitoring the uptake of fluorescent glucose analogue 2-NBDG in concert with glucose consumption and lactate secretion in vitro. WT Th17 cells were highly glycolytic, showing increased glucose uptake when compared with naive T cells. Consistent with the normal expression of the main proglycolytic molecules in the absence of PKM2 expression, glucose uptake by PKM2-deficient Th17 cells was not different from that of WT Th17 cells, even in the presence of IL-23 (Fig. 3E and Fig. S2E).

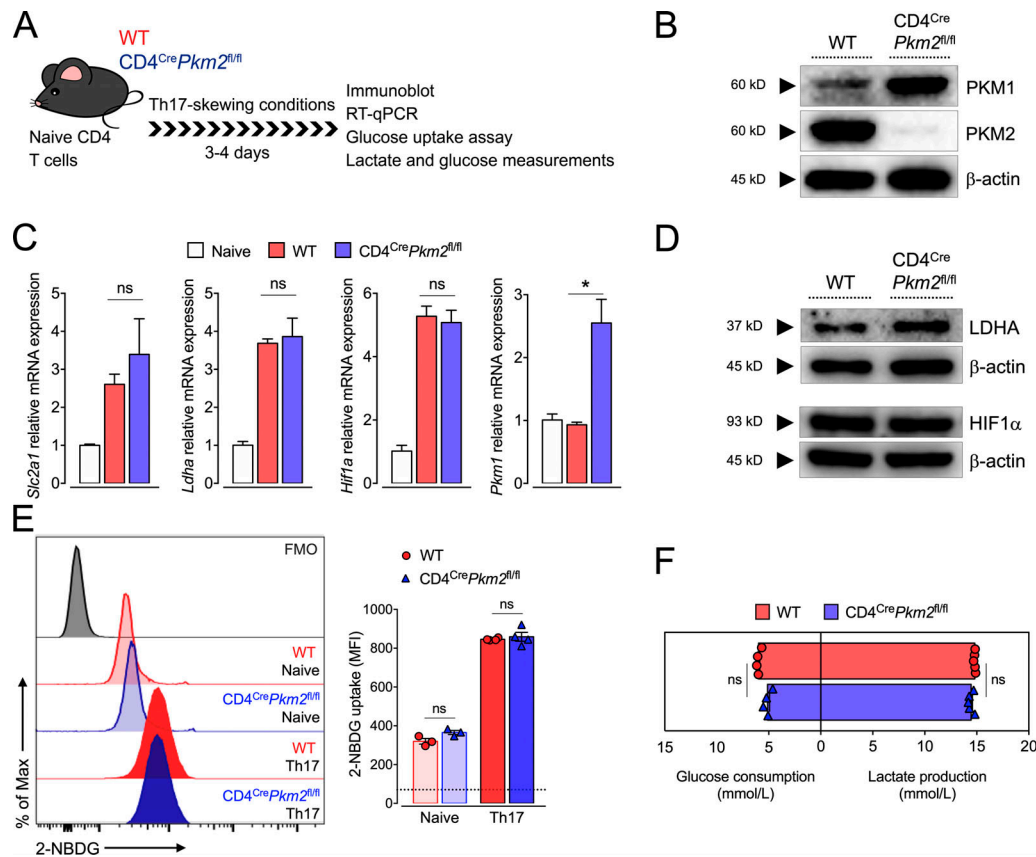


Figure 3. PKM2 deficiency does not alter Th17 cell metabolic reprogramming. (A) Naive CD4 T cells were obtained from CD4^{Cre}*Pkm2*^{fl/fl} or control littermates (WT) and cultured under Th17 cell-skewing conditions. (B) PKM1 protein expression in PKM2-deficient Th17 cells was determined by immunoblot; PKM2 deficiency was also confirmed by immunoblot analysis. (C) Th17 cells were harvested to evaluate the expression of glycolysis-related genes (*Slc2a1*, *Ldha*, *Hif1a*, and *Pkm1*) by RT-qPCR; data were normalized to *Gapdh* and fold change calculated relative to freshly isolated naive CD4 T cells (*n* = 3). (D) WT and PKM2-deficient Th17 cells were harvested at 96 h to determine protein levels of LDHA and HIF1 α by immunoblot. β -Actin was used as loading control. (E) Th17 cells were incubated with a fluorescent glucose analogue (2-NBDG; 30 μ M) for glucose uptake evaluation by flow cytometry; dotted lines indicate fluorescence-minus-one (FMO) control values (*n* = 3–4). MFI, mean fluorescence intensity. (F) Glucose consumption and lactate production were measured in Th17 cell-culture supernatants (*n* = 4–5). Data are representative of two (D, E and F) or three (B and C) independent experiments. Error bars show mean \pm SEM. P values were determined by one-way ANOVA followed by Tukey's post hoc test (C), two-way ANOVA followed by Tukey's post hoc test (E), or two-tailed Student's *t* test (F). *, *P* < 0.05; ns, not significant.

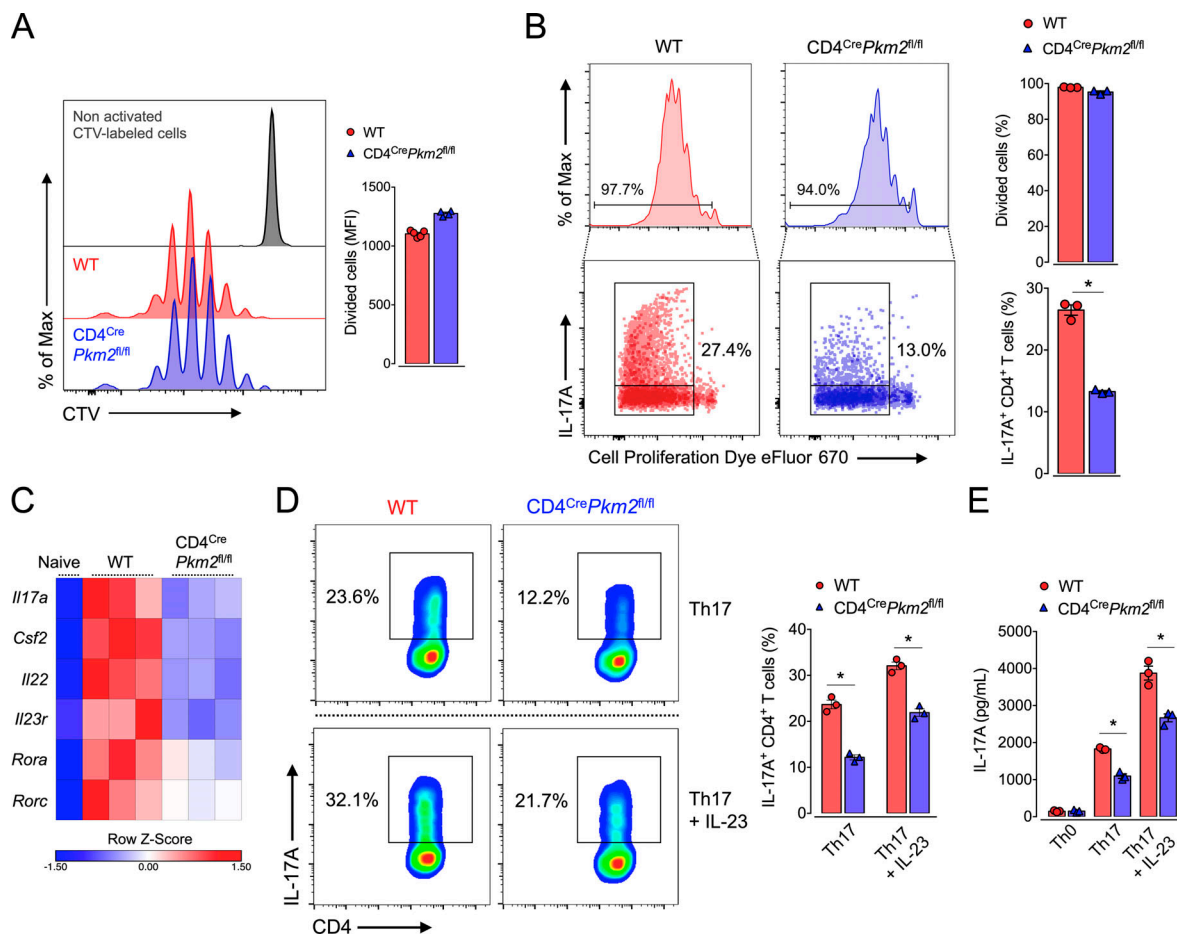


Figure 4. PKM2 deficiency impairs Th17 cell differentiation. (A) Naive CD4 T cells from WT or conditional knockout (CD4^{Cre}Pkm2^{fl/fl}) mice were stained with CellTrace Violet proliferation dye (CTV; 5 μ M). Cells were then cultured under Th17 cell-skewing conditions and after 96 h cell proliferation was evaluated by flow cytometry; MFI, mean fluorescence intensity ($n = 5$). (B) Cells were stained with 5 μ M eFluor 670 proliferation dye and cultured under Th17 cell-polarizing conditions for 96 h. Cells were intracellularly stained for IL-17A after 4 h of PMA/ionomycin stimulation ($n = 3$). (C) The expression of Th17 cell-signature genes was evaluated by RT-qPCR and displayed in a heatmap. Gene expression correlates with color intensity, data normalized by Z-score (row); cycle threshold values were normalized to *Gapdh* ($n = 3$). (D) Naive CD4 T cells from WT or CD4^{Cre}Pkm2^{fl/fl} were also differentiated in the presence of IL-23 and frequency of IL-17A⁺ CD4 T cell population determined by flow cytometry ($n = 3$). (E) Supernatants of Th17 cultures were collected, and IL-17A levels detected were by ELISA ($n = 3$). Data are representative of two (A–C) or more than five (D and E) independent experiments. Error bars indicate mean \pm SEM. P values were determined by two-way ANOVA followed by Tukey's post hoc test (D and E) or two-tailed Student's *t* test (A and B). *, $P < 0.05$.

Moreover, glucose consumption and lactate production were not significantly different between WT and PKM2-deficient Th17 cells (Fig. 3 F and Fig. S2 F). Collectively, these results indicate that PKM2 deficiency did not impair the metabolic reprogramming of Th17 cells toward aerobic glycolysis.

To assess whether loss of PKM2 function affects T cells proliferative capacity, we next performed flow cytometric analysis of fluorescent dye dilution in CD4 T cells stimulated with anti-CD3 ϵ and anti-CD28 in the presence of Th17 cell-polarizing cytokines. PKM2-deficient CD4 T cells showed normal proliferative capacity after 72 h in culture (Fig. 4 A). Additionally, we evaluated the proliferation of PKM2-deficient T cells cultured under a Th0 condition, and again no significant differences were detected, even in the presence of IL-2 (Fig. S2 G). However, proliferating PKM2-deficient Th17 cells showed significantly reduced expression of IL-17A (Fig. 4 B), suggesting that PKM2 is required for differentiation, but not Th17 cell proliferation. Consistent with this association, expression of the Th17 cell-

related genes *Il17a*, *Csf2*, *Il22*, *Il23r*, *Rora*, and *Rorc* were also markedly reduced in PKM2-deficient Th17 cells (Fig. 4 C). Further analysis confirmed that PKM2 deficiency impaired rises in IL-17A expression in Th17 cells, even after they had been differentiated in the presence of IL-23 (Fig. 4, D and E). Nevertheless, reduced IL-17A expression was not accompanied by alteration of Foxp3 expression in PKM2-deficient Th17 cells (Fig. S3 A). Moreover, PKM2 deficiency did not affect Th1, Th2, or iT reg cell differentiation (Fig. S3, B–D), suggesting that Th17 differentiation requires PKM2, whereas the differentiation of other Th cell subtypes is unaffected by the loss of PKM2 function in vitro.

Loss of PKM2 in T cells ameliorates autoimmune-mediated neuroinflammation

To determine the in vivo relevance of these findings, we next examined whether the loss of PKM2 in T cells influenced the pathogenesis of EAE. To this end, CD4^{Cre}Pkm2^{fl/fl} mice were

immunized with MOG₃₅₋₅₅ peptide. Notably, the loss of PKM2 in T cells not only significantly reduced the clinical severity but also decreased the incidence of EAE (Fig. 5, A–C). Consistently, histopathological analysis with H&E and fluoromyelin staining of spinal cords showed that CD4^{Cre}Pkm2^{fl/fl} mice had lower inflammatory cell infiltration and decreased demyelination than WT mice (Fig. 5 D). To evaluate the impact of PKM2 deficiency on Th17 differentiation during EAE, we next analyzed the expression of Th17 cell-associated genes in DLNs. Deficiency of PKM2 in T cells resulted in a significant reduction of the Th17 cell-related genes *Il17a*, *Rora*, and *Rorc* in DLNs before disease onset (day 6; Fig. 5 E), suggesting that T cell-specific deletion of PKM2 inhibits Th17 cell differentiation in the EAE model. Indeed, loss of PKM2 in T cells significantly reduced the frequency of IL-17A⁺ CD4 T cells in DLNs at the peak of the disease (day 15), whereas the population of Foxp3⁺ CD4 T cells remained unaltered (Fig. S4 A). Moreover, when we restimulated cells isolated from DLNs of EAE mice with MOG₃₅₋₅₅ ex vivo, the frequency of IL-17A⁺Roryt⁺ CD4 T cells and the production of IL-17A, GM-CSF, and IFN- γ by PKM2-deficient T cells were significantly lower compared to WT cells (Fig. 5 F and Fig. S4 B). PKM2 deficiency also reduced the transcription of mature pathogenic Th17 cell effector genes *Csf2* and *Ifng* in the total spinal cord tissue at the peak of EAE symptoms (Fig. S4 C). Consistent with this, mRNA transcription levels in *Pkm2* and Th17 cell-related genes, including *Il17a*, *Il21*, *Csf2*, *Ifng*, *Il23r*, *Rora*, and *Rorc*, were lower in CD4 T cells isolated from the spinal cords of CD4^{Cre}Pkm2^{fl/fl} mice than in those obtained from WT mice (Fig. 5 G). Accordingly, mice lacking PKM2 in T cells had significantly decreased frequencies of IL-17A⁺ CD4 T cells coproducing the pathogenic Th17 cytokines GM-CSF or IFN γ in their spinal cords (Fig. 5 H). Of note, we noticed that deficiency of PKM2 did not affect the frequency of IFN γ ⁺GM-CSF⁺ Th1 cells in vitro, while the generation of IL-17A⁺GM-CSF⁺ Th17 cells was impaired (Fig. S3 E).

To further confirm the role of PKM2 for the development of encephalitogenic Th17 cells, we adoptively transferred enriched MOG-specific WT or PKM2-deficient Th17 cells in vitro into *Rag1*^{-/-} mice. We found that the loss of PKM2 in Th17 cells significantly reduced their ability to induce passive EAE when compared with WT cells (Fig. S4 D). Collectively, these data indicate that PKM2 is required for Th17 cell differentiation in vitro and in vivo, contributing to the pathogenesis of EAE.

PKM2 promotes STAT3 phosphorylation in Th17 cells

In its tetrameric form, PKM2 has high metabolic activity converting phosphoenolpyruvate to pyruvate in the glycolytic pathway. However, its less enzymatically active dimeric form has the potential to translocate into the nucleus and act as a transcriptional coactivator (Yang et al., 2011; Gao et al., 2012). In this context, phosphorylation of PKM2 at tyrosine 105 (Y105) prevents tetramer conformation, favoring the dimeric state (Hitosugi et al., 2009). To investigate how PKM2 regulates Th17 cell differentiation, we initially examined its phosphorylation status and conformational state. We found that increases in total PKM2 expression preceded parallel increases in its phosphorylation at Y105 during Th17 cell differentiation, peaking at 72 h of culture (Fig. 6 A). Phosphorylated PKM2 at Y105 was also

increased in the spinal cord tissue of EAE mice and was positively associated with the clinical score of the disease (Fig. S4 E). Moreover, immunoblot analysis of protein cross-linking assay revealed that all oligomeric forms of PKM2 were up-regulated in Th17 cells when compared with Th0 cells after 72 h of culture. However, the dimeric PKM2 was the most prevalent conformation detected, mainly when Th17 cells were differentiated in the presence of IL-23 (Fig. 6 B), suggesting that PKM2 can be translocated into the nucleus. Indeed, confocal immunofluorescence microscopy analysis revealed a punctate staining pattern of PKM2 in Th17 cells, with both cytoplasmic and nuclear localization, whereas Th0 cells showed an evenly distributed pattern of PKM2 mainly in the cytoplasm (Fig. 6 C). Immunoblot analysis of cytoplasmic and nuclear fractions further confirmed the nuclear translocation of PKM2 in Th17 cells (Fig. 6 D).

To investigate the functional importance of the PKM2 nuclear translocation in mediating Th17 cell differentiation, we next used the small molecule TEPP-46, which is a well-characterized PKM2-specific allosteric activator that promotes tetramer formation and inhibits nuclear translocation (Anastasiou et al., 2012). Notably, treating CD4 T cells with TEPP-46 significantly reduced Th17 cell differentiation to the same level as that observed in PKM2-deficient T cells (Fig. 6 E and Fig. S5 A), suggesting that dimeric PKM2 nuclear translocation is required for the regulation of Th17 cell differentiation. Indeed, immunoblot analysis of nuclear fractions of Th17 cells showed that TEPP-46 completely abrogated the translocation of PKM2 into the nucleus (Fig. 6 F). Of note, we found that PKM2 also translocates into the nucleus of Th1 cells, which is also inhibited by TEPP-46 (Fig. S5 B). Nevertheless, TEPP-46 did not affect the differentiation of Th1 cells (Fig. S5 C).

IL-6 and IL-23 induce Th17 cell differentiation through activation of the STAT3 signaling (Korn et al., 2009; Dong, 2008). Moreover, the phosphorylation of STAT3 (phospho-STAT3) at Y705 residue is known to be required for Th17 cell differentiation (Guanizo et al., 2018; Renner et al., 2008). Interestingly, the nuclear dimeric PKM2 form can act as a protein kinase and phosphorylate STAT3 at Y705 in the nucleus, enhancing its transcriptional activity and promoting tumor growth (Gao et al., 2012). We then examined whether PKM2 and STAT3 proteins can interact during the differentiation of Th17 cells. Confocal immunofluorescence images indicated that STAT3 and PKM2 colocalize in the nucleus of Th17 cells (Fig. 7 A). Indeed, immunoprecipitation coupled to immunoblot analysis showed that PKM2 coimmunoprecipitated with STAT3 in WT Th17 cells (Fig. 7 B). The specific PKM2–STAT3 interaction was supported by immunoprecipitating STAT3 in PKM2-deficient Th17 cells and using a control IgG antibody for the immunoprecipitation assay. To further confirm the direct interaction between PKM2 and STAT3, we also conducted a proximity ligation assay (PLA) in Th17 cells. We found a robust fluorescent signal generated by PLA probes targeting STAT3 and PKM2 in WT, but not PKM2-deficient, Th17 cells, indicating a nuclear PKM2–STAT3 interaction (Fig. 7 C and Fig. S5 D).

We then evaluated whether the absence of PKM2 could affect the phosphorylation status of STAT3. Immunoblot analysis demonstrated that acute phosphorylation of STAT3 at Y705 by

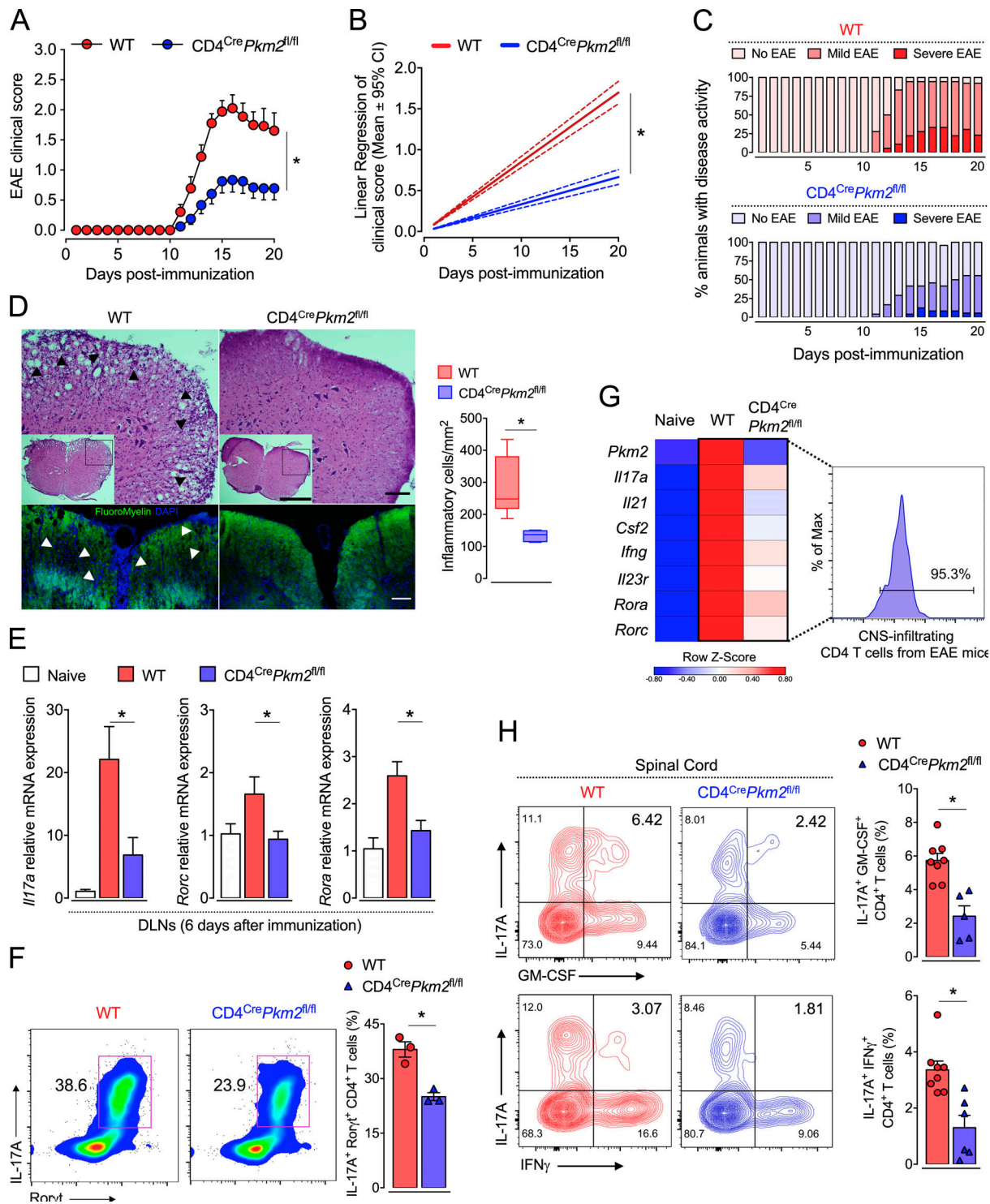


Figure 5. T cell-specific PKM2 deletion ameliorates autoimmune-mediated inflammation. (A–C) WT or $CD4^{Cre}Pkm2^{fl/fl}$ mice were immunized with MOG_{35–55} and monitored daily for clinical signs ($n = 18–24$ per group). (A) Cumulative EAE clinical scores. (B) Representation by linear regression curves; dashed lines indicate the 95% confidence intervals. (C) Disease incidence by severity is represented on a bar chart as no EAE (score <1), mild EAE (score 1–2), and severe EAE (score ≥ 2.5). (D) Inflammatory cell infiltration in the spinal cord (top; black arrowheads) was observed by using H&E staining; the number of inflammatory cells in transverse spinal cord sections was determined in a blinded fashion (right; $n = 7$ per group). Scale bars represent 500 and 50 μ m. Fluoromyelin staining (green) was performed to detect demyelination sites (bottom; white arrowheads); nuclei labeled with DAPI (blue). Scale bar indicates 50 μ m. (E) Analysis of *Il17a*, *Rora*, and *Rorc* gene expression in DLN cells collected 6 d after immunization. Data were normalized to *Gapdh*; fold-change is relative to naive controls ($n = 5$ per group). (F) DLN cells were harvested 6 d after immunization and restimulated in vitro with MOG_{35–55}; the frequencies of IL-17A⁺Ror γ t⁺ CD4⁺ T cells were then determined by flow cytometry ($n = 3$). (G) CNS-infiltrating CD4 T cells were isolated. Each sample was a pool of cells from two mice and analyzed for expression of Th17 cell-associated genes ($n = 6$ per group). Cycle threshold values were normalized to *Gapdh*; fold change is relative to CNS CD45⁺ cells from naive mice. Data were normalized by Z score (row) and depicted in a heatmap. (H) Spinal cord-infiltrating mononuclear cells were collected from WT

and $CD4^{Cre}Pkm2^{fl/fl}$ mice 15 d after immunization for flow cytometric analysis of IL-17A⁺ CD4 T cell populations coproducing GM-CSF or IFN γ ($n = 5-8$ per group). Data are pooled from three (A-C) or representative of two (E-H) or three (D) independent experiments. Error bars represent mean \pm SEM. P values were determined by one-way ANOVA followed by Tukey's post hoc test (E), two-way ANOVA followed by Tukey's post hoc test (A and B), or two-tailed Student's t test (D, F and H). *, $P < 0.05$.

IL-6 stimulation was reduced in TCR-activated PKM2-deficient CD4 T cells when compared with WT CD4 T cells (Fig. 7 D). Additionally, fully differentiated PKM2-deficient Th17 cells (96 h culture) showed significantly lower levels of phosphorylated STAT3 at Y705, while the total STAT3 protein expression was not altered (Fig. 7 E and Fig. S5 E). In accordance, TEPP-46 also substantially reduced the levels of nuclear Y705-phosphorylated

STAT3 in Th17 cells (Fig. 7 F). Of note, although the abundance of phosphorylated STAT3 in Th1 cells is markedly lower than that observed in Th17 cells, PKM2-deficient Th1 cells showed reduced levels of phosphorylated STAT3 when compared with WT cells (Fig. S5 E). In vivo, the deficiency of PKM2 in T cells resulted in a significant reduction of Y705-phosphorylated STAT3 in the spinal cord tissue of EAE mice compared to

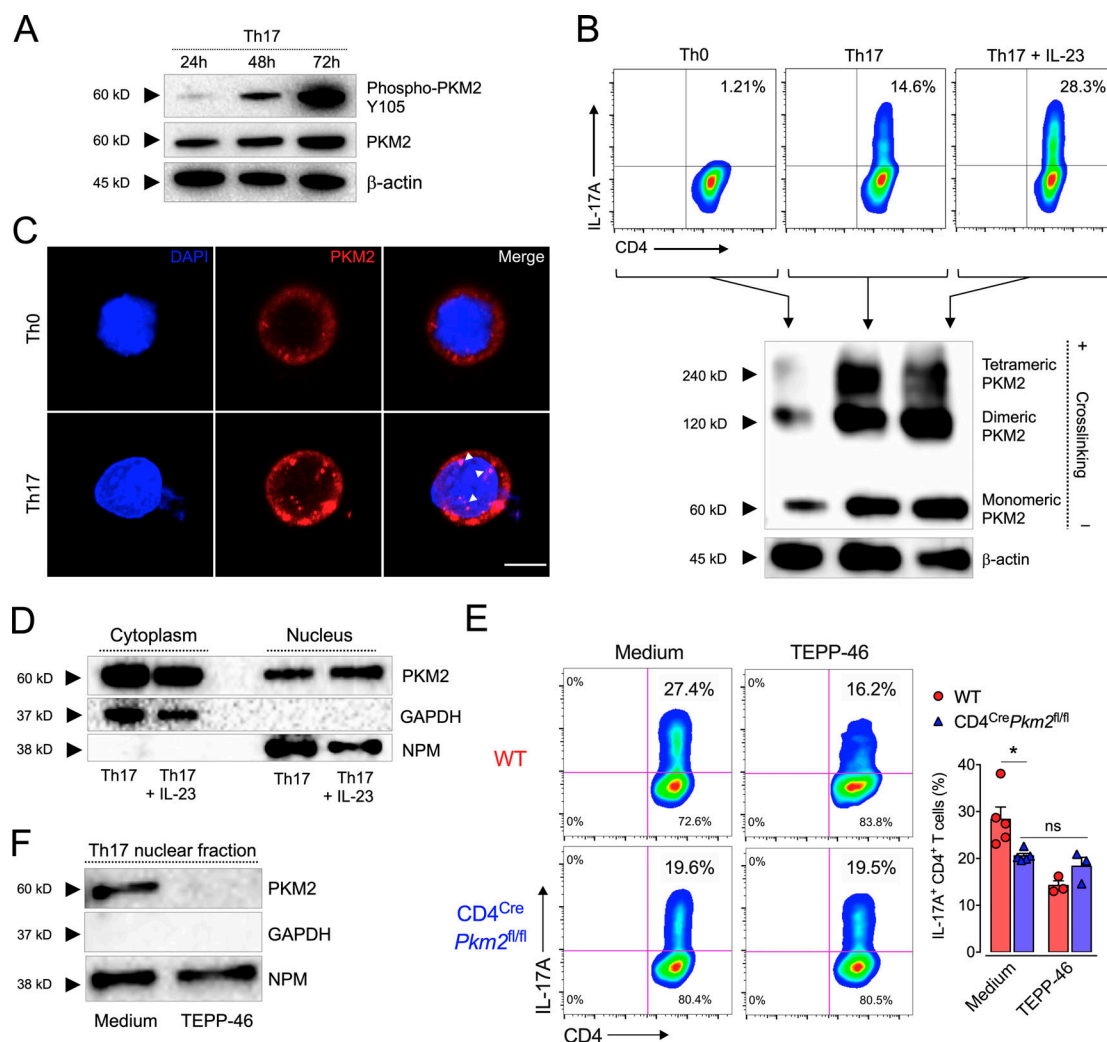


Figure 6. PKM2 translocates into the nucleus of Th17 cells. (A) The degree of PKM2 phosphorylation at Y105 was determined by immunoblot at different time points of Th17 cell culture; β -actin was used as a loading control. (B) Th0 or Th17 cells underwent protein cross-linking using disuccinimidyl suberate followed by immunoblot analysis to identify PKM2 oligomer states. (C) Naive CD4 T cells were cultured under Th17 cell-inducing conditions for 96 h and prepared for confocal immunofluorescence analysis. Cells were stained with fluorophore-conjugated anti-PKM2 (red) and nuclei labeled with DAPI (blue). Confocal images were acquired; scale bar indicates 5 μ m. (D) Cytoplasmic and nuclear protein extracts from Th17 cell culture were obtained and analyzed by immunoblot to determine PKM2 levels in these compartments. GAPDH and NPM were used as cytoplasm and nuclear loading controls, respectively. (E) WT or PKM2-deficient CD4 T cells were cultured under Th17 cell-skewing conditions in the presence of or absence of TEPP-46 (100 μ M), a PKM2 activator, followed by flow cytometry analysis of IL-17A⁺ CD4 T cells frequencies ($n = 3-5$). (F) Nuclear fractions from Th17 cells were obtained and analyzed by immunoblot to determine PKM2 protein expression. GAPDH and NPM were used as cytoplasm and nuclear loading controls, respectively. Data are representative of two independent experiments. Error bars are mean \pm SEM. P values were determined by two-way ANOVA followed by Tukey's post hoc test (E). *, $P < 0.05$.

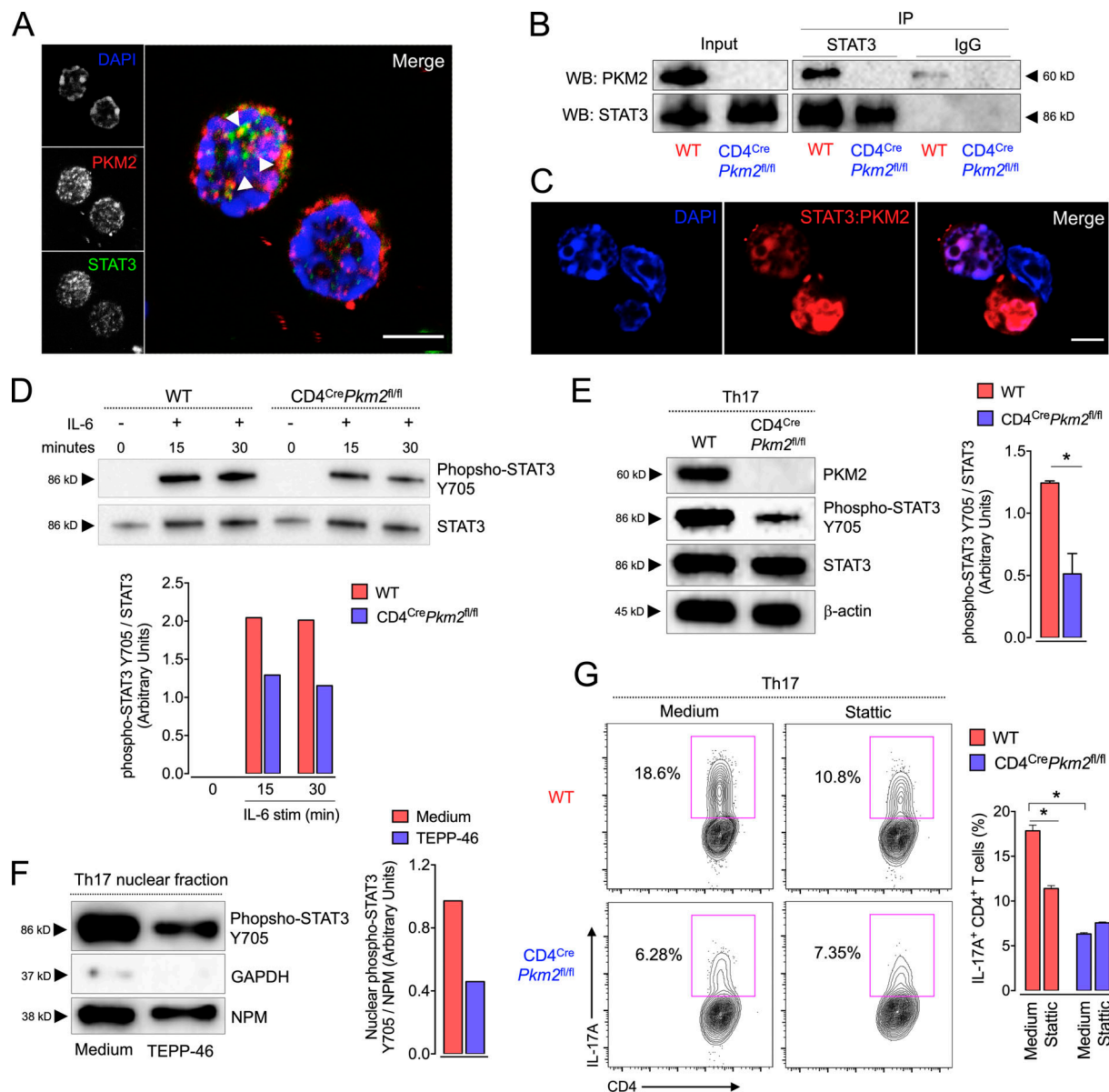


Figure 7. Nuclear PKM2 regulates STAT3 activation in Th17 cells. (A) Immunofluorescence staining of intracellular PKM2 (red) and STAT3 (green) was performed in differentiated Th17 cells; nuclei were labeled with DAPI (blue). Confocal analysis was used for image acquisition. Scale bar represents 5 μ m. (B) The interaction between STAT3 and PKM2 was examined by immunoprecipitation (IP). Briefly, Th17 cell lysates were subjected to IP with a mouse anti-STAT3 or control IgG antibody, followed by immunoblot analysis using a rabbit anti-PKM2 and anti-STAT3. Protein extracts without immunoprecipitation (input) served as positive controls. WB, Western blot. (C) PLA was performed to detect the interaction between PKM2 and STAT3 (in red) in differentiated Th17 cells. The blue signal indicates DAPI-stained nuclei. Confocal images were acquired; scale bar represents 5 μ m. (D) WT or PKM2-deficient naive CD4 T cells were activated with anti-CD3 ϵ :CD28 for 48 h. Cells were then acutely stimulated with recombinant mouse IL-6 (10 ng/ml) and collected 15 or 30 min later for immunoblot analysis. (E) Immunoblot was performed to identify total and phosphorylated (Y705) levels of STAT3 in WT or PKM2-deficient Th17 cells; β -actin was used as the loading control. (F) Immunoblot analysis of nuclear fraction from Th17 cells to determine phosphorylated STAT3 (Y705) protein expression. GAPDH and NPM were used as cytoplasm and nuclear loading controls, respectively. (G) Statistic (2 μ M), an inhibitor of STAT3 activation, was added to Th17 cell cultures for 96 h, followed by flow cytometric analysis ($n = 3$). Data are representative of two (A–D, F, and G) or four (E) independent experiments. Error bars show mean \pm SEM. P values were determined by two-way ANOVA followed by Tukey's post hoc test (G) or two-tailed Student's t test (E). *, $P < 0.05$.

WT mice (Fig. S5 F). Finally, we examined the importance of STAT3 activation by PKM2 in the differentiation of Th17 cells. To this end, we investigated the effect of a suboptimal concentration of Statistic, a small-molecule inhibitor of STAT3 activation (Schust et al., 2006), on the differentiation of Th17 cells. As expected, a suboptimal concentration of Statistic partially reduced the differentiation of WT Th17 cells, whereas it

had no additive inhibition on the Th17 differentiation observed in PKM2-deficient T cells (Fig. 7 G). Of note, the inhibition of STAT3 activation did not affect Th1 cell differentiation in WT or PKM2-deficient T cells (Fig. S5 G). Taken together, our results provide strong evidence for the nonmetabolic role of PKM2 in the Th17 cell differentiation program.

Discussion

Recent studies connecting the fields of cellular metabolism and immunology have dramatically improved our understanding of how immune cells benefit from a metabolic reprogramming to support their activation, proliferation, and differentiation (O'Neill et al., 2016; Buck et al., 2015; Almeida et al., 2016). Emerging evidence proposes that metabolic enzymes, rather than solely being components of biochemical pathways, are also proteins that mediate many other biological functions, including gene transcription and cell cycle progression (Yu and Li, 2017; Seki and Gaultier, 2017). The enzyme PK is a critical rate-limiting enzyme in the glycolytic pathway that catalyzes the formation of pyruvate from phosphoenolpyruvate. Notably, the PK isoform M2 is not only present in the cytoplasm as a metabolic enzyme but also can translocate into the nucleus, indicating that it has additional noncanonical or nonmetabolic functions unrelated to glycolysis (Israelsen and Vander Heiden, 2015; Gui et al., 2013).

In the present study, we have shown that PKM2 acts as a transcriptional coactivator during Th17 cell differentiation by fine-tuning STAT3 nuclear activation. We have shown that PKM2 is hardly detectable in naive T cells, whereas the TCR activation of T cells substantially increases its expression, at least in part, through mTORC1 signaling. mTORC1 is a well-known metabolic sensor that promotes aerobic glycolysis by inducing the expression of several glycolysis-related genes (Saxton and Sabatini, 2017). Consistent with our results, it has been previously reported that the mTORC1–HIF1 α signaling axis up-regulates the expression of PKM2 in tumor cells (Sun et al., 2011; Iqbal et al., 2013). Importantly, T cell-specific deletion of mTORC1 activity or HIF1 α impairs Th17 differentiation (Delgoffe et al., 2011; Kurebayashi et al., 2012; Shi et al., 2011; Dang et al., 2011). In this context, we found that PKM2 mRNA and protein expression are higher in differentiated Th17 cells than other Th cell subtypes. Consistent with this, we found that CD4 T cells isolated from the spinal cords of mice undergoing EAE, a well-characterized animal autoimmune disease model for the effector function of Th17 cells (Sie et al., 2014), express high levels of PKM2 in parallel with the up-regulation of the Th17 cell-related genes *Il17a*, *Csf2*, *Il23r*, *Rora*, and *Rorc*. This association implies a potential role of this glycolytic enzyme in supporting Th17 cell differentiation. It is noteworthy that while we did not detect alteration in *Pkm1* mRNA levels throughout Th17 cell differentiation, we observed a particular increase in PKM1 protein levels in fully differentiated Th17 cells, which might result from reduced proteasomal degradation. Thus, it will be important to determine if the later up-regulation PKM1 expression is solely part of the differentiation process or a response to the metabolic demand of mature Th17 cells.

PKM2 acts as a transcriptional coactivator for β -catenin and HIF1 α in tumor cells, promoting the expression of genes involved in glycolysis and proliferation (Yang et al., 2011; Luo et al., 2011). Moreover, LPS-induced glycolytic reprogramming and IL-1 β production by macrophages require nuclear interaction of PKM2 with HIF1 α (Palsson-McDermott et al., 2015). We therefore hypothesized that PKM2 would also be required for the metabolic reprogramming and proliferation of Th17 cells. Strikingly, PKM2 deficiency neither impaired the metabolic

reprogramming toward aerobic glycolysis nor affected the proliferative capacity of Th17 cells. Nonetheless, the loss of PKM2 in T cells selectively inhibited Th17 differentiation without altering Th1, Th2, or iT reg cell differentiation in vitro.

As described above, the neuroinflammation observed in mice undergoing EAE is mainly mediated by autoantigen-specific Th17 cells (Sie et al., 2014). Consistent with our in vitro results, the specific loss of PKM2 in T cells not only significantly reduced the clinical severity but also decreased the incidence of EAE. These declines were associated with a lower frequency of IL-17A⁺ CD4 T cells and less Th17 cell-related cytokine production by T cells upon ex vivo stimulation with MOG_{35–55}. Nevertheless, while we did not find a role for PKM2 in Th1 cell polarization in vitro, mice lacking PKM2 in T cells showed a reduced frequency of T cells expressing IFN γ during EAE. A plausible explanation for these last findings is the potential conversion of Th17 cells into IL-17A⁺IFN γ ⁺ CD4 T cells, which is one of the signatures of pathogenic Th17 cells and the dominant T cell population found in the spinal cord of EAE mice (Kurschus et al., 2010; Hirota et al., 2011). In support of this, we also demonstrated that GM-CSF, another pathogenic Th17 cell signature cytokine (Codarri et al., 2011; El-Behi et al., 2011), was similarly reduced in mice lacking PKM2 in T cells during EAE. However, cytokine-driven T cell polarization in vitro is different from pathophysiological differentiation in vivo, where other mediators might be directly or indirectly involved. Thus, we cannot rule out the possibility that PKM2 might regulate Th1 cell differentiation in vivo. Indeed, it was reported that homocysteine stimulation of T cells increases glycolytic metabolism and IFN- γ expression in a PKM2-dependent manner (Lü et al., 2018).

In agreement with our findings, during the revision process of this article, a study was published supporting the role of PKM2 in the generation of Th17 cells (Kono et al., 2019). However, using shikonin, a pharmacological inhibitor of PKM2, it was proposed that inhibition of PKM2 impairs Th17 cell differentiation by reducing glycolysis, which contrasts with our metabolic findings obtained with the genetic approach (Cre/LoxP). The differences in the metabolic profile might be explained by off-target effects of shikonin in other enzymes that regulate glycolysis, including the inhibition of glycogen synthase kinase 3 β (GSK-3 β) and cell division cycle 25 (Cdc25) phosphatases (Chen et al., 2019; Zhang et al., 2019; Liang et al., 2016). Furthermore, we found that the deficiency of PKM2 in Th17 cells led to a compensatory up-regulation of PKM1 expression, which might explain the normal glycolytic profile that we have observed and also supports the hypothesis of a nonmetabolic mechanism of PKM2 in mediating Th17 cell differentiation. The differential role of PKM1 in Th17 cell differentiation is currently unclear and merits further investigation.

PKM1 and PKM2 isoforms are products of alternative splicing of the same *Pkm* gene (Noguchi et al., 1986). PKM2, in its tetrameric form, has high metabolic activity in the glycolysis pathway, similar to PKM1. However, the less enzymatically active dimeric form of PKM2 can translocate into the nucleus and act as a transcriptional coactivator (Yang et al., 2011; Luo et al., 2011; Yang et al., 2012a). Phosphorylation of PKM2 on Y105 is indicative of the dimeric form of PKM2, as it prevents the

tetrameric conformation (Hitosugi et al., 2009). Herein, we found that the expression of total PKM2 was followed by increased phosphorylation at Y105 during Th17 cell differentiation. Consistently, the dimeric form of PKM2 was the most prevalent conformation detected in Th17 cells, localized in both cytoplasmic and nuclear compartments. Other posttranslational modifications of PKM2, including acetylation and succinylation, have been reported to affect PKM2 conformation favoring the dimeric form (Lv et al., 2013; Wang et al., 2017). Therefore, we cannot exclude the role of other posttranslational modifications affecting the translocation of PKM2 into the nucleus of Th17 cells. However, consistent with the well-characterized effect of small compound TEPP-46 in promoting PKM2 tetramer formation and inhibiting its nuclear translocation (Anastasiou et al., 2012), we observed that TEPP-46 reduces Th17 cell differentiation, suggesting that nuclear translocation of PKM2 is required for the generation of Th17 cells. Indeed, this hypothesis was recently supported by Angiari et al. (2020). Since the nuclear translocation of PKM2 requires the binding of its nuclear localization signal sequence to the importin $\alpha 5$, an adaptor protein that imports proteins into the nucleus (Yang et al., 2012b), further analysis showing the interaction of the PKM2 nuclear localization signal with importin $\alpha 5$ in Th17 cells may help to confirm our conclusions.

Nuclear PKM2 has been shown to interact with and enhance STAT3 phosphorylation at Y705, contributing to increases in cancer cell proliferation (Gao et al., 2012) and inflammatory cytokine production by macrophages (Shirai et al., 2016). Moreover, it was reported that the mutation of PKM2 at residue R399 locks it in dimeric conformation, enhancing its ability to phosphorylate STAT3 (Gao et al., 2012). In this context, it is well known that IL-6 and IL-23 promote differentiation of Th17 cells through activation of the STAT3 signaling pathway (Korn et al., 2009; Dong, 2008). Interestingly, integrative phosphoproteomics analysis of IL-23-activated T cells revealed predominant phosphorylation of preexisting STAT3 nuclear subsets in addition to the translocation of phosphorylated STAT3 (Lochmatter et al., 2016). In the current study, we demonstrated that PKM2 interacts with STAT3 in the nucleus of Th17 cells, and deficiency or inhibition of nuclear translocation of PKM2 significantly reduced phosphorylation of STAT3 levels in Th17 cells. Whether the observed phosphorylation of STAT3 is due to direct phosphorylation catalyzed by the nuclear dimeric PKM2 or caused by an indirect mechanism via another protein kinase needs to be further investigated. Of note, the potential role of nuclear PKM2 as a protein kinase has been recently debated (Hosios et al., 2015).

In conclusion, we have demonstrated that PKM2 acts as a critical nonmetabolic regulator of Th17 cell differentiation by enhancing the activation of STAT3 (Fig. 8). Our study also highlights the role of PKM2 in the regulation of pathogenic Th17 cells during autoimmune-mediated neuroinflammation. PKM2, therefore, may represent a potential therapeutic target for autoimmune-mediated inflammation.

Materials and methods

Mice

C57BL/6, CD4^{Cre} (Tg(Cd4-Cre)1Cwi/Bfl/J; Lee et al., 2001), *Pkm2*^{fllox} (B6;129S-Pkmtm1.1Mgvh/J; Israelsen et al., 2013), and *Rag1*^{-/-} mice

were purchased from Jackson Laboratories. Conditional knockout mice (CD4^{Cre}*Pkm2*^{fl/fl}) were generated by crossing CD4^{Cre} to *Pkm2*^{fllox} mice, which were maintained on a C57BL/6 genetic background. All animals were housed in a specific pathogen-free facility at the Ribeirao Preto Medical School under controlled temperature (22–25°C) and 12-h light-dark cycle and provided with water and food ad libitum. Mice used in experiments were sex and age matched. All experiments were performed in accordance with protocols approved by the Ethics Committee on Animal Use of Ribeirao Preto Medical School, University of São Paulo.

In vitro T cell differentiation

Naive CD4⁺CD25⁻ T cells were purified from LNs and spleen of WT C57BL/6, CD4^{Cre}*Pkm2*^{fl/fl} or control littermate (CD4^{Cre} and *Pkm2*^{fl/fl}) mice with the untouched CD4 T cell isolation kit (Miltenyi Biotec) and a biotinylated CD25 monoclonal antibody (eBioscience) by using an AutoMACS magnetic cell sorter (Miltenyi Biotec) according to the manufacturer's protocol. Purified cells were activated with soluble anti-CD3 ϵ :CD28 (both 1 μ g/ml; BD Biosciences) on U-bottomed plates (10⁵/well). Skewing conditions were as follows: Th17, 2.5 ng/ml rhTGF- β 1 (eBioscience) plus 20 ng/ml rmIL-6 (R&D Systems) with or without 20 ng/ml rmIL-23 (R&D Systems); Th1, rmIL-12, and rmIL-2 (both 20 ng/ml; R&D Systems); Th2, anti-IFN- γ (10 μ g/ml), rmIL-4, and rmIL-2 (both 20 ng/ml; R&D Systems). For iT reg cell polarization, naive T cells were cultured with plate-bound CD3 ϵ :CD28 (both 1 μ g/ml; BD Biosciences) in the presence of 1 ng/ml rhTGF- β 1 (eBioscience). When indicated, 0.1 μ M rapamycin (Cayman Chemical), 100 μ M TEPP-46 (Millipore), or 2 μ M Stattic (Tocris) was used.

Induction and assessment of EAE

EAE was induced by subcutaneously immunizing mice in the flanks with MOG_{35–55} (Proteimax). The 300 μ g of administered MOG_{35–55} was composed of 100 μ l PBS and 100 μ l CFA (Sigma-Aldrich) supplemented with 5 mg/ml heat-inactivated *Mycobacterium tuberculosis* H37Ra (Difco). Additionally, mice received 200 ng pertussis toxin (Sigma-Aldrich) i.p. followed on the day of immunization as well as 2 d later. For adoptive transfer experiments, DLNs cells were harvested from WT or CD4^{Cre}*Pkm2*^{fl/fl} donor 8 d after immunization and cultured in vitro with MOG_{35–55} under Th17 cell-polarizing conditions for 72 h. CD4 T cells were isolated by magnetic separation (Miltenyi Biotec), and a total of 10⁶ CD4 T cells were injected i.v. into naive *Rag1*^{-/-} recipients. 1 d later, the recipient mice were immunized with MOG_{35–55} plus pertussis toxin, as previously described. Clinical signs of EAE were scored on a standard 0–5 scale, according to previous recommendations (Stromnes and Goverman, 2006), as follows: 0 = unaffected; 0.5 = partial limp tail; 1 = paralyzed tail; 1.5 = loss of coordinated movements; 2 = hindlimb paresis; 2.5 = one hindlimb paralyzed; 3 = both hindlimbs paralyzed; 3.5 = hindlimbs paralyzed and weakness in forelimbs; 4 = one forelimb paralyzed; 4.5 = both forelimbs paralyzed; and 5 = moribund/death.

RNA isolation and quantitative real-time PCR (RT-qPCR)

Total RNA from cultures or sorted CD4 T cells were isolated using the RNeasy Isolation Kit according to the manufacturer's instructions (Qiagen). Total RNA from spinal cords was harvested

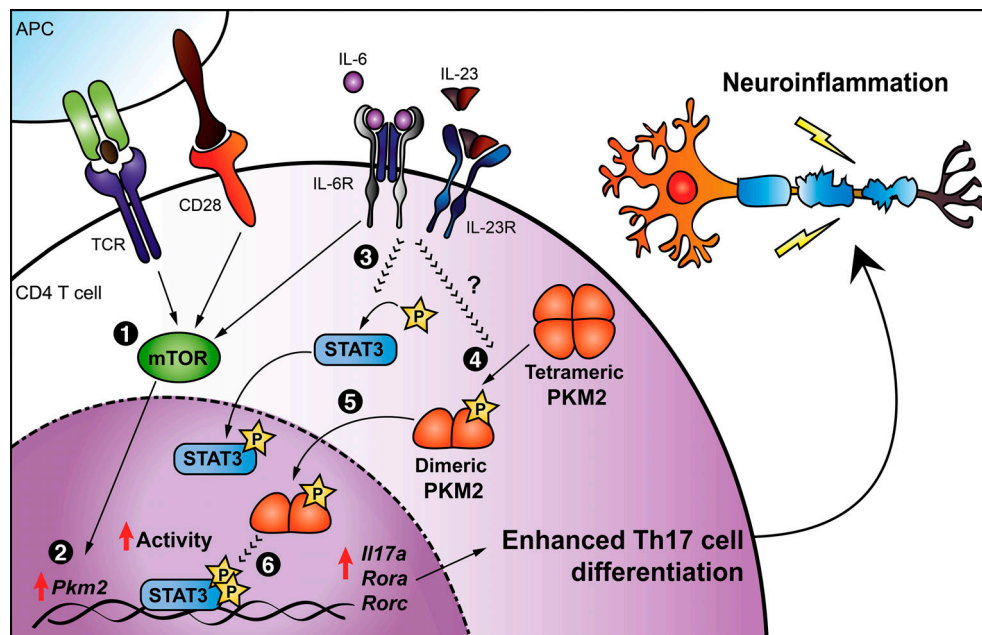


Figure 8. Schematic representation describing how PKM2 induces Th17 cell differentiation. The cooperation between TCR activation and costimulatory signals per se leads to a significant increase of *Pkm2* expression (1), which is highly augmented by the presence of IL-6 and IL-23, important cytokines for controlling the Th17 cell phenotype program. This cascade boosts the activity of the metabolic sensor mTOR that, in turn, contributes to *Pkm2* transcription (2). IL-6R and IL-23R signaling cascade promote STAT3 phosphorylation/activation (3), concomitantly with an accumulation of PKM2 dimers in Th17 cells (4). The dimeric oligomer state facilitates PKM2 translocation into the nucleus (5) and its interaction with STAT3, increasing its transcriptional activity (6). This process culminates in enhanced transcription of Th17 cell-associated genes, contributing to the development of autoimmune neuroinflammation.

following the TRIzol Reagent (Invitrogen) protocol. The RNA was quantified and then converted to cDNA using the High Capacity cDNA Reverse Transcription Kit (Applied Biosystems). RT-qPCR was performed with SYBR Green PCR Master Mix (Applied Biosystems) using a StepOnePlus Real-Time PCR machine (Applied Biosystems). Gene expression was determined relative to *Gapdh* and fold change calculated by using the $2^{-\Delta\Delta CT}$ threshold cycle method. In some cases, gene expression was represented as heatmaps generated by using the open-source software Morpheus (<https://software.broadinstitute.org/morpheus>). A list of primers is presented in Table S1.

Flow cytometry

For intracellular cytokine staining, cells were stimulated in culture medium with PMA (50 ng/ml; Sigma-Aldrich) and ionomycin (500 ng/ml; Sigma-Aldrich) for 4 h in the presence of monensin (GolgiStop 1.5 μ g/ml; BD Biosciences) at 37°C in a humidified 5% CO₂ chamber. The cells were then washed and stained for 10 min at room temperature with fixable viability dye (Invitrogen) for dead cells exclusion and fluorochrome-labeled monoclonal antibodies against surface cell markers. Afterward, cells were fixed and permeabilized using Cytofix/Cytoperm (BD Biosciences) and Perm/Wash buffer (BD Biosciences), followed by intracellular staining with monoclonal antibodies for 20 min. Intracellular staining of transcription factors was done without stimulation, with the eBioscience Foxp3 Fixation/Permeabilization Kit. Data were acquired on FACSVerse or FACSCanto II machines (BD Biosciences) and analyzed using FlowJo software (Tree Star).

Cell proliferation assay

Naive CD4⁺CD25⁻ T cells were labeled with Cell Proliferation Dye eFluor 670 or CellTrace Violet (both 5 μ M; Invitrogen) following the manufacturer's protocol. Cells were then resuspended in culture medium and activated with anti-CD3 ϵ :CD28 (both 1 μ g/ml; BD Biosciences) in the presence or absence of rmIL-2 (20 ng/ml; R&D Systems) or cultured under Th17 cell-skewing conditions for 3 d. The stepwise dilution of the fluorescence in daughter cells as indicative of cell proliferation was assessed by flow cytometry.

Cytokine measurement

Supernatants from cell cultures were collected after centrifugation and IFN- γ , IL-17A, GM-CSF, and IL-13 levels were measured by ELISA according to the manufacturer's instructions (R&D Systems).

Glucose uptake, consumption, and lactate production

For flow cytometry-based glucose uptake assay, naive CD4 T cells or differentiated Th17 cells were stimulated (1 μ g/ml anti-CD3 ϵ :CD28) and incubated with 30 μ M 2-NBDG (Invitrogen), a fluorescent glucose analogue, diluted in the glucose-free medium for 30 min at 37°C before measuring fluorescence by flow cytometry. Lactate and glucose concentrations in the cell culture supernatants were measured with colorimetric kit assays according to the manufacturer's instructions (Bioclin).

Immunoprecipitation and immunoblot analysis

Whole-cell lysates were prepared using radioimmunoprecipitation assay lysis buffer (Sigma-Aldrich) supplemented with

protease and phosphatase inhibitor cocktail (Cell Signaling). Protein concentrations were determined with a bicinchoninic acid protein assay reagent kit (Sigma-Aldrich). For separation by electrophoresis, 10 μ g total protein was loaded onto SDS-polyacrylamide gels according to standard protocols (SDS-PAGE) and then transferred to nitrocellulose membrane (GE Healthcare). Membranes were blocked with 5% (wt/vol) nonfat milk (Cell Signaling) in Tris-buffered saline with 0.1% Tween-20 (TBST) for 1 h at room temperature and then incubated overnight at 4°C with 1:1,000 dilutions of primary antibodies against PKM1, PKM2, phospho-PKM2 (Y105), STAT3, phospho-STAT3 (Y705), LDHA, or HIF1 α (all from Cell Signaling). Subsequently, membranes were repeatedly washed with TBST and incubated for 2 h with the appropriate HRP-conjugated secondary antibody (1:5,000 dilution; Sigma-Aldrich). Immunoreactivity was detected using the ECL prime reagent (GE Healthcare), and then the chemiluminescence signal was recorded on the ChemiDoc XRS Imager (Bio-Rad Laboratories). Data were analyzed with Image Lab software (Bio-Rad Laboratories). Total β -actin levels were used as a loading control. Immunoprecipitation was performed using the Pierce coIP kit (Thermo Scientific) following the manufacturer's protocol. Briefly, control IgG antibody and mouse anti-STAT3 (Cell Signaling) were immobilized using AminoLink Plus coupling resin. Equal amounts of Th17 cell lysates were pre-cleared and subsequently incubated with the antibody-coupled resin overnight at 4°C. Afterward, the resin was washed, and proteins were eluted using elution buffer. The immunoprecipitated samples were analyzed for PKM2 and STAT3 protein expression by immunoblot, as described above.

Subcellular fractionation

Nuclear and cytosolic fractionation was performed by using the NE-PER Nuclear and Cytoplasmic Extraction Reagents kit according to the manufacturer's recommendations (Thermo Scientific). Protein levels were quantified (bicinchoninic acid) and samples separated by SDS-PAGE before immunoblot analysis. The housekeeping proteins GAPDH and nucleophosmin (NPM) were used as cytosolic and nuclear loading controls, respectively.

Cross-linking reaction

Th0 cells (no cytokines) or differentiated Th17 cells were cross-linked with 500 μ M disuccinimidyl suberate (Sigma-Aldrich) for 30 min, and then cell lysates were prepared with radioimmunoprecipitation assay buffer. The subsequent steps were performed as described in the immunoblot analysis section.

Antigen-specific T cell response

Cells from DLNs and spleen of EAE-bearing mice were isolated and cultured in 96-well round-bottom plates (3×10^5 cells/well) with MOG_{35–55} (50 μ g/ml) in culture medium for 4 d at 37°C. The concentration of IL-17A, GM-CSF, and IFN- γ in the culture supernatants was measured using ELISA kits (R&D Systems).

Preparation of central nervous system (CNS) mononuclear cells

EAE mice were deeply anesthetized and transcardially perfused with ice-cold PBS. The spinal cord was collected and minced

with a sharp razor blade, following digestion for 30 min at 37°C with collagenase D (2.5 mg/ml; Roche Diagnostics). Mononuclear cells were isolated by the passage of the tissue through a cell strainer (70 μ m), followed by centrifugation through a 37/70% Percoll gradient (GE Healthcare). For intracellular cytokine staining, isolated cells were stimulated as previously described, followed by flow cytometric analysis. Conversely, cell suspensions were labeled with anti-CD4 (L3T4) microbeads (Miltenyi Biotec) and separated using an AutoMACS magnetic cell sorter (Miltenyi Biotec). The purity of cell preparations was >90%, and total RNA was extracted for RT-qPCR analysis.

Histology

Mice were anesthetized and perfused with cold PBS, followed by 4% paraformaldehyde (PFA). Spinal cords were collected, post-fixed in 4% PFA, and then cryoprotected in 30% sucrose solution for 72 h. Tissues were then embedded in OCT compound (Tissue-Tek; Sakura Finetek) and snap-frozen on dry ice. Spinal cords were cryostat-cut (Leica) into 20- μ m-thick transverse sections, mounted on glass slides, and stained with H&E. A pathologist assessed transverse spinal cord tissue sections for inflammatory cell infiltration in a blinded fashion.

Immunofluorescence

For immunofluorescence analysis, spinal cord cryosections were permeabilized with 0.2% Triton X-100 in PBS for 20 min, blocked with 2% BSA in PBS for 30 min, and then incubated overnight at 4°C with primary antibodies. Subsequently, sections were incubated for 2 h at room temperature with species-specific Alexa Fluor-conjugated secondary antibodies (Abcam). CNS tissue sections were incubated for 1 h with the fluorescent myelin stain FluoroMyelin Green (1:200; Invitrogen). Slides were rinsed in PBS and coverslipped in ProLong Gold antifade reagent with DAPI (Invitrogen). For T cell immunofluorescence, cells were incubated on poly-L-lysine-coated coverslips, fixed (4% PFA), and permeabilized. After incubation with primary and secondary antibodies, coverslips were washed and mounted onto microscope slides using a DAPI-containing mounting medium. The following primary antibodies were used: anti-PKM2 (1:200; Abcam) and anti-STAT3 (1:200; Cell Signaling). The slides were visualized with a high-resolution SP5 confocal microscope (Leica) and image analysis performed on Fiji software.

PLA

PLA was performed using a Duolink In Situ Kit Mouse/Rabbit according to the manufacturer's instructions (Sigma-Aldrich). Briefly, Naive CD4 T cells were cultured under Th17 cell-skewing conditions for 96 h. Cells were attached to poly-L-lysine-coated cover slides, fixed with 2% PFA (10 min at room temperature), washed with PBS, and blocked with blocking buffer (30 min at room temperature). Cells were permeabilized (0.1% Triton X-100) and intracellularly stained with primary mouse anti-STAT3 and rabbit anti-PKM2 (overnight at 4°C; both from Cell Signaling), followed by incubation with oligonucleotide-labeled secondary antibodies. Ligase was added for the hybridization of PLA probes (30 min at 37°C) to form a circularized DNA strand if in close proximity. Samples were incubated

with amplification solution containing fluorescently labeled oligonucleotides plus polymerase (100 min at 37°C) for the rolling-circle amplification reaction. Fluorescent signals indicating proximity was visualized by confocal microscopy.

Statistical analysis

GraphPad Prism 7.0 software was used for statistical analysis. Multiple-group comparisons were performed with either one-way ANOVA or two-way ANOVA followed by Tukey's post hoc test. Unpaired two-tailed Student's *t* test was used for comparison of two conditions. Data are expressed as means \pm SEM. *P* value < 0.05 was considered significant.

Online supplemental material

Fig. S1 validates the expression of signature genes of CD4 T cell subsets and exhibits the differential expression of *Pkml* and *Pkm2* among naive, effector/memory, and Th17 cells, and it also shows the PKM2 protein levels in Th1 and Th17 cells. **Fig. S2** includes data showing that T cell-specific PKM2 deletion in mice does not cause gross defect and present data reinforcing that loss of PKM2 does not affect glucose uptake, lactate production, and proliferation of CD4 T cells. **Fig. S3** demonstrates that loss of PKM2 in CD4 T cells does not impair Th1, Th2, or iT reg cell differentiation. **Fig. S4** displays additional data confirming that PKM2 boosts Th17 cell-mediated EAE pathogenesis. **Fig. S5** shows that both STAT3 activation and PKM2 are dispensable for Th1 differentiation and provide data showing reduced levels of STAT3 activation in the spinal cord of EAE PKM2-deficient mice. Table S1 contains the sequences of mouse primer pairs used for RT-qPCR analysis. Table S2 lists the reagents used in the study.

Acknowledgments

We thank all members of the Laboratory of Inflammation and Pain at Ribeirao Preto Medical School for technical support and discussions.

This work was supported by São Paulo Research Foundation grant 2013/08216-2 (Center for Research in Inflammatory Diseases) and National Council for Scientific and Technological Development grant 430823/2018-5. This work was also supported by São Paulo Research Foundation fellowships for L.E.A. Damasceno (2016/10280-9), D.S. Prado (16/05377-3), J.E. Toller-Kawahisa (17/01714-8), and M.H. Rosa (18/23910-6).

Author contributions: L.E.A. Damasceno, D.S. Prado, F.P. Veras, F.Q. Cunha, T.M. Cunha, and J.C. Alves-Filho designed experiments and provided conceptual input. L.E.A. Damasceno, D.S. Prado, F.P. Veras, M.M. Fonseca, J.E. Toller-Kawahisa, M.H. Rosa, G.A. Públio, and T.V. Martins performed experiments. A. Waisman provided reagents. L.E.A. Damasceno, D.S. Prado, F.P. Veras, F.S. Ramalho, and J.C. Alves-Filho analyzed data. L.E.A. Damasceno and J.C. Alves-Filho wrote the manuscript.

Disclosures: The authors declare no competing interests exist.

Submitted: 5 April 2019

Revised: 28 May 2019

Accepted: 28 May 2020

References

- Almeida, L., M. Lochner, L. Berod, and T. Sparwasser. 2016. Metabolic pathways in T cell activation and lineage differentiation. *Semin. Immunol.* 28:514–524. <https://doi.org/10.1016/j.smim.2016.10.009>
- Anastasiou, D., Y. Yu, W.J. Israelsen, J.-K. Jiang, M.B. Boxer, B.S. Hong, W. Tempel, S. Dimov, M. Shen, A. Jha, et al. 2012. Pyruvate kinase M2 activators promote tetramer formation and suppress tumorigenesis. *Nat. Chem. Biol.* 8:839–847. <https://doi.org/10.1038/nchembio.1060>
- Angiari, S., M.C. Runtsch, C.E. Sutton, E.M. Pålsson-McDermott, B. Kelly, N. Rana, H. Kane, G. Papadopoulou, E.L. Pearce, K.H.G. Mills, et al. 2020. Pharmacological Activation of Pyruvate Kinase M2 Inhibits CD4⁺ T Cell Pathogenicity and Suppresses Autoimmunity. *Cell Metab.* 31:391–405.e8. <https://doi.org/10.1016/j.cmet.2019.10.015>
- Bettelli, E., Y. Carrier, W. Gao, T. Korn, T.B. Strom, M. Oukka, H.L. Weiner, and V.K. Kuchroo. 2006. Reciprocal developmental pathways for the generation of pathogenic effector TH17 and regulatory T cells. *Nature.* 441:235–238. <https://doi.org/10.1038/nature04753>
- Buck, M.D., D. O'Sullivan, and E.L. Pearce. 2015. T cell metabolism drives immunity. *J. Exp. Med.* 212:1345–1360. <https://doi.org/10.1084/jem.20151159>
- Chen, Z., A. Laurence, Y. Kanno, M. Pacher-Zavisin, B.-M. Zhu, C. Tato, A. Yoshimura, L. Hennighausen, and J.J. O'Shea. 2006. Selective regulatory function of Socs3 in the formation of IL-17-secreting T cells. *Proc. Natl. Acad. Sci. USA.* 103:8137–8142. <https://doi.org/10.1073/pnas.0600666103>
- Chen, Y., Z.Y. Chen, L. Chen, J.Y. Zhang, L.Y. Fu, L. Tao, Y. Zhang, X.X. Hu, and X.C. Shen. 2019. Shikonin inhibits triple-negative breast cancer-cell metastasis by reversing the epithelial-to-mesenchymal transition via glycogen synthase kinase 3 β -regulated suppression of β -catenin signaling. *Biochem. Pharmacol.* 166:33–45. <https://doi.org/10.1016/j.bcp.2019.05.001>
- Christofk, H.R., M.G. Vander Heiden, M.H. Harris, A. Ramanathan, R.E. Gerszten, R. Wei, M.D. Fleming, S.L. Schreiber, and L.C. Cantley. 2008. The M2 splice isoform of pyruvate kinase is important for cancer metabolism and tumour growth. *Nature.* 452:230–233. <https://doi.org/10.1038/nature06734>
- Codarri, L., G. Gyölvézi, V. Tosevski, L. Hesske, A. Fontana, L. Magnenat, T. Suter, and B. Becher. 2011. ROR γ t drives production of the cytokine GM-CSF in helper T cells, which is essential for the effector phase of autoimmune neuroinflammation. *Nat. Immunol.* 12:560–567. <https://doi.org/10.1038/ni.2027>
- Dang, E.V., J. Barbi, H.-Y. Yang, D. Jinasena, H. Yu, Y. Zheng, Z. Bordman, J. Fu, Y. Kim, H.-R. Yen, et al. 2011. Control of T(H)17/T(reg) balance by hypoxia-inducible factor 1. *Cell.* 146:772–784. <https://doi.org/10.1016/j.cell.2011.07.033>
- Delgoffe, G.M., K.N. Pollizzi, A.T. Waickman, E. Heikamp, D.J. Meyers, M.R. Horton, B. Xiao, P.F. Worley, and J.D. Powell. 2011. The kinase mTOR regulates the differentiation of helper T cells through the selective activation of signaling by mTORC1 and mTORC2. *Nat. Immunol.* 12:295–303. <https://doi.org/10.1038/ni.2005>
- Dong, C.. 2008. TH17 cells in development: an updated view of their molecular identity and genetic programming. *Nat. Rev. Immunol.* 8:337–348. <https://doi.org/10.1038/nri2295>
- El-Behi, M., B. Ciric, H. Dai, Y. Yan, M. Cullimore, F. Safavi, G.-X. Zhang, B.N. Dittel, and A. Rostami. 2011. The encephalitogenicity of T(H)17 cells is dependent on IL-1- and IL-23-induced production of the cytokine GM-CSF. *Nat. Immunol.* 12:568–575. <https://doi.org/10.1038/ni.2031>
- Gao, X., H. Wang, J.J. Yang, X. Liu, and Z.-R. Liu. 2012. Pyruvate kinase M2 regulates gene transcription by acting as a protein kinase. *Mol. Cell.* 45: 598–609. <https://doi.org/10.1016/j.molcel.2012.01.001>
- Guanizo, A.C., C.D. Fernando, D.J. Garama, and D.J. Gough. 2018. STAT3: a multifaceted oncoprotein. *Growth Factors.* 36:1–14. <https://doi.org/10.1080/08977194.2018.1473393>
- Gui, D.Y., C.A. Lewis, and M.G. Vander Heiden. 2013. Allosteric regulation of PKM2 allows cellular adaptation to different physiological states. *Sci. Signal.* 6:pe7–pe7. <https://doi.org/10.1126/scisignal.2003925>
- Hirota, K., J.H. Duarte, M. Veldhoen, E. Hornsby, Y. Li, D.J. Cua, H. Ahlfors, C. Wilhelm, M. Tolaini, U. Menzel, et al. 2011. Fate mapping of IL-17-producing T cells in inflammatory responses. *Nat. Immunol.* 12:255–263. <https://doi.org/10.1038/ni.1993>
- Hitosugi, T., S. Kang, M.G. Vander Heiden, T.-W. Chung, S. Elf, K. Lythgoe, S. Dong, S. Lonial, X. Wang, G.Z. Chen, et al. 2009. Tyrosine phosphorylation inhibits PKM2 to promote the Warburg effect and tumor growth. *Sci. Signal.* 2:ra73–ra73. <https://doi.org/10.1126/scisignal.2000431>
- Hosios, A.M., B.P. Fiske, D.Y. Gui, and M.G. Vander Heiden. 2015. Lack of Evidence for PKM2 Protein Kinase Activity. *Mol. Cell.* 59:850–857. <https://doi.org/10.1016/j.molcel.2015.07.013>

- Iqbal, M.A., F.A. Siddiqui, V. Gupta, S. Chattopadhyay, P. Gopinath, B. Kumar, S. Manvati, N. Chaman, and R.N.K. Bamezai. 2013. Insulin enhances metabolic capacities of cancer cells by dual regulation of glycolytic enzyme pyruvate kinase M2. *Mol. Cancer*. 12:72. <https://doi.org/10.1186/1476-4598-12-72>
- Israelsen, W.J., and M.G. Vander Heiden. 2015. Pyruvate kinase: Function, regulation and role in cancer. *Semin. Cell Dev. Biol.* 43:43–51. <https://doi.org/10.1016/j.semcdb.2015.08.004>
- Israelsen, W.J., T.L. Dayton, S.M. Davidson, B.P. Fiske, A.M. Hosios, G. Bellinger, J. Li, Y. Yu, M. Sasaki, J.W. Horner, et al. 2013. PKM2 isoform-specific deletion reveals a differential requirement for pyruvate kinase in tumor cells. *Cell*. 155:397–409. <https://doi.org/10.1016/j.cell.2013.09.025>
- Ivanov, I.I., B.S. McKenzie, L. Zhou, C.E. Tadokoro, A. Lepelletier, J.J. Lafaille, D.J. Cua, and D.R. Littman. 2006. The orphan nuclear receptor RORgammat directs the differentiation program of proinflammatory IL-17+ T helper cells. *Cell*. 126:1121–1133. <https://doi.org/10.1016/j.cell.2006.07.035>
- Kono, M., K. Maeda, I. Stocton-Gavanescu, W. Pan, M. Umeda, E. Katsuyama, C. Burbano, S.Y.K. Orite, M. Vukelic, M.G. Tsokos, et al. 2019. Pyruvate kinase M2 is requisite for Th1 and Th17 differentiation. *JCI Insight*. 4. e127395. <https://doi.org/10.1172/jci.insight.127395>
- Korn, T., E. Bettelli, M. Oukka, and V.K. Kuchroo. 2009. IL-17 and Th17 Cells. *Annu. Rev. Immunol.* 27:485–517. <https://doi.org/10.1146/annurev.immunol.021908.132710>
- Kurebayashi, Y., S. Nagai, A. Ikejiri, M. Ohtani, K. Ichiyama, Y. Baba, T. Yamada, S. Egami, T. Hoshii, A. Hirao, et al. 2012. PI3K-Akt-mTORC1-S6K1/2 axis controls Th17 differentiation by regulating Gfi1 expression and nuclear translocation of RORγ. *Cell Rep.* 1:360–373. <https://doi.org/10.1016/j.celrep.2012.02.007>
- Kurschus, F.C., A.L. Croxford, A.P. Heinen, S. Wörtge, D. Ielo, and A. Waisman. 2010. Genetic proof for the transient nature of the Th17 phenotype. *Eur. J. Immunol.* 40:3336–3346. <https://doi.org/10.1002/eji.201040755>
- Lee, P.P., D.R. Fitzpatrick, C. Beard, H.K. Jessup, S. Lehar, K.W. Makar, M. Pérez-Melgosa, M.T. Sweetser, M.S. Schlissel, S. Nguyen, et al. 2001. A critical role for Dnmt1 and DNA methylation in T cell development, function, and survival. *Immunity*. 15:763–774. [https://doi.org/10.1016/S1074-7613\(01\)00227-8](https://doi.org/10.1016/S1074-7613(01)00227-8)
- Liang, J., R. Cao, Y. Zhang, Y. Xia, Y. Zheng, X. Li, L. Wang, W. Yang, and Z. Lu. 2016. PKM2 dephosphorylation by Cdc25A promotes the Warburg effect and tumorigenesis. *Nat. Commun.* 7:12431. <https://doi.org/10.1038/ncomms12431>
- Lochmatter, C., R. Fischer, P.D. Charles, Z. Yu, F. Powrie, and B.M. Kessler. 2016. Integrative Phosphoproteomics Links IL-23R Signaling with Metabolic Adaptation in Lymphocytes. *Sci. Rep.* 6:24491. <https://doi.org/10.1038/srep24491>
- Lü, S., J. Deng, H. Liu, B. Liu, J. Yang, Y. Miao, J. Li, N. Wang, C. Jiang, Q. Xu, et al. 2018. PKM2-dependent metabolic reprogramming in CD4+ T cells is crucial for hyperhomocysteinemia-accelerated atherosclerosis. *J. Mol. Med. (Berl.)*. 96:585–600. <https://doi.org/10.1007/s00109-018-1645-6>
- Luo, W., H. Hu, R. Chang, J. Zhong, M. Knabel, R. O'Meally, R.N. Cole, A. Pandey, and G.L. Semenza. 2011. Pyruvate kinase M2 is a PHD3-stimulated coactivator for hypoxia-inducible factor 1. *Cell*. 145:732–744. <https://doi.org/10.1016/j.cell.2011.03.054>
- Lv, L., Y.-P. Xu, D. Zhao, F.-L. Li, W. Wang, N. Sasaki, Y. Jiang, X. Zhou, T.-T. Li, K.-L. Guan, et al. 2013. Mitogenic and oncogenic stimulation of K433 acetylation promotes PKM2 protein kinase activity and nuclear localization. *Mol. Cell*. 52:340–352. <https://doi.org/10.1016/j.molcel.2013.09.004>
- Mangan, P.R., L.E. Harrington, D.B. O'Quinn, W.S. Helms, D.C. Bullard, C.O. Elson, R.D. Hatton, S.M. Wahl, T.R. Schoeb, and C.T. Weaver. 2006. Transforming growth factor-β induces development of the T(H)17 lineage. *Nature*. 441:231–234. <https://doi.org/10.1038/nature04754>
- McGeachy, M.J., Y. Chen, C.M. Tato, A. Laurence, B. Joyce-Shaikh, W.M. Blumenschein, T.K. McClanahan, J.J. O'Shea, and D.J. Cua. 2009. The interleukin 23 receptor is essential for the terminal differentiation of interleukin 17-producing effector T helper cells in vivo. *Nat. Immunol.* 10:314–324. <https://doi.org/10.1038/ni.1698>
- Noguchi, T., H. Inoue, and T. Tanaka. 1986. The M1- and M2-type isozymes of rat pyruvate kinase are produced from the same gene by alternative RNA splicing. *J. Biol. Chem.* 261:13807–13812.
- O'Neill, L.A.J., R.J. Kishton, and J. Rathmell. 2016. A guide to immunometabolism for immunologists. *Nat. Rev. Immunol.* 16:553–565. <https://doi.org/10.1038/nri.2016.70>
- Palsson-McDermott, E.M., A.M. Curtis, G. Goel, M.A.R. Lauterbach, F.J. Sheedy, L.E. Gleeson, M.W.M. van den Bosch, S.R. Quinn, R. Domingo-Fernandez, D.G.W. Johnston, et al. 2015. Pyruvate kinase M2 regulates Hif-1α activity and IL-1β induction and is a critical determinant of the warburg effect in LPS-activated macrophages. *Cell Metab.* 21:65–80. <https://doi.org/10.1016/j.cmet.2014.12.005>
- Qin, H., L. Wang, T. Feng, C.O. Elson, S.A. Niyongere, S.J. Lee, S.L. Reynolds, C.T. Weaver, K. Roarty, R. Serra, et al. 2009. TGF-β promotes Th17 cell development through inhibition of SOCS3. *J. Immunol.* 183:97–105. <https://doi.org/10.4049/jimmunol.0801986>
- Renner, E.D., S. Rylaarsdam, S. Añover-Sombke, A.L. Rack, J. Reichenbach, J.C. Carey, Q. Zhu, A.F. Jansson, J. Barboza, L.F. Schimke, et al. 2008. Novel signal transducer and activator of transcription 3 (STAT3) mutations, reduced T(H)17 cell numbers, and variably defective STAT3 phosphorylation in hyper-IgE syndrome. *J. Allergy Clin. Immunol.* 122:181–187. <https://doi.org/10.1016/j.jaci.2008.04.037>
- Saxton, R.A., and D.M. Sabatini. 2017. mTOR Signaling in Growth, Metabolism, and Disease. *Cell*. 168:960–976. <https://doi.org/10.1016/j.cell.2017.02.004>
- Schust, J., B. Sperl, A. Hollis, T.U. Mayer, and T. Berg. 2006. Stattic: a small-molecule inhibitor of STAT3 activation and dimerization. *Chem. Biol.* 13:1235–1242. <https://doi.org/10.1016/j.chembiol.2006.09.018>
- Seki, S.M., and A. Gaultier. 2017. Exploring Non-Metabolic Functions of Glycolytic Enzymes in Immunity. *Front. Immunol.* 8:1549. <https://doi.org/10.3389/fimmu.2017.01549>
- Shi, L.Z., R. Wang, G. Huang, P. Vogel, G. Neale, D.R. Green, and H. Chi. 2011. HIF1α-dependent glycolytic pathway orchestrates a metabolic checkpoint for the differentiation of TH17 and Treg cells. *J. Exp. Med.* 208:1367–1376. <https://doi.org/10.1084/jem.20110278>
- Shirai, T., R.R. Nazarewicz, B.B. Wallis, R.E. Yanes, R. Watanabe, M. Hillhorst, L. Tian, D.G. Harrison, J.C. Giacomini, T.L. Assimes, et al. 2016. The glycolytic enzyme PKM2 bridges metabolic and inflammatory dysfunction in coronary artery disease. *J. Exp. Med.* 213:337–354. <https://doi.org/10.1084/jem.20150900>
- Sie, C., T. Korn, and M. Mitsdoerffer. 2014. Th17 cells in central nervous system autoimmunity. *Exp. Neurol.* 262(Pt A):18–27. <https://doi.org/10.1016/j.expneurol.2014.03.009>
- Stromnes, I.M., and J.M. Goverman. 2006. Active induction of experimental allergic encephalomyelitis. *Nat. Protoc.* 1:1810–1819. <https://doi.org/10.1038/nprot.2006.285>
- Sun, Q., X. Chen, J. Ma, H. Peng, F. Wang, X. Zha, Y. Wang, Y. Jing, H. Yang, R. Chen, et al. 2011. Mammalian target of rapamycin up-regulation of pyruvate kinase isoenzyme type M2 is critical for aerobic glycolysis and tumor growth. *Proc. Natl. Acad. Sci. USA*. 108:4129–4134. <https://doi.org/10.1073/pnas.1014769108>
- Veldhoen, M., R.J. Hocking, C.J. Atkins, R.M. Locksley, and B. Stockinger. 2006. TGFβ in the context of an inflammatory cytokine milieu supports de novo differentiation of IL-17-producing T cells. *Immunity*. 24:179–189. <https://doi.org/10.1016/j.immuni.2006.01.001>
- Wang, F., K. Wang, W. Xu, S. Zhao, D. Ye, Y. Wang, Y. Xu, L. Zhou, Y. Chu, C. Zhang, et al. 2017. SIRT5 Desuccinylates and Activates Pyruvate Kinase M2 to Block Macrophage IL-1β Production and to Prevent DSS-Induced Colitis in Mice. *Cell Rep.* 19:2331–2344. <https://doi.org/10.1016/j.celrep.2017.05.065>
- Yang, X.O., A.D. Panopoulos, R. Nurieva, S.H. Chang, D. Wang, S.S. Watowich, and C. Dong. 2007. STAT3 regulates cytokine-mediated generation of inflammatory helper T cells. *J. Biol. Chem.* 282:9358–9363. <https://doi.org/10.1074/jbc.C600321200>
- Yang, X.O., B.P. Pappu, R. Nurieva, A. Akimzhanov, H.S. Kang, Y. Chung, L. Ma, B. Shah, A.D. Panopoulos, K.S. Schluns, et al. 2008. T helper 17 lineage differentiation is programmed by orphan nuclear receptors RORα and RORγ. *Immunity*. 28:29–39. <https://doi.org/10.1016/j.immuni.2007.11.016>
- Yang, W., Y. Xia, H. Ji, Y. Zheng, J. Liang, W. Huang, X. Gao, K. Aldape, and Z. Lu. 2011. Nuclear PKM2 regulates β-catenin transactivation upon EGFR activation. *Nature*. 480:118–122. <https://doi.org/10.1038/nature0598>
- Yang, W., Y. Xia, D. Hawke, X. Li, J. Liang, D. Xing, K. Aldape, T. Hunter, W.K. Alfred Yung, and Z. Lu. 2012a. PKM2 phosphorylates histone H3 and promotes gene transcription and tumorigenesis. *Cell*. 150:685–696. <https://doi.org/10.1016/j.cell.2012.07.018>
- Yang, W., Y. Zheng, Y. Xia, H. Ji, X. Chen, F. Guo, C.A. Lyssiotis, K. Aldape, L.C. Cantley, and Z. Lu. 2012b. ERK1/2-dependent phosphorylation and nuclear translocation of PKM2 promotes the Warburg effect. *Nat. Cell Biol.* 14:1295–1304. <https://doi.org/10.1038/ncb2629>
- Yang, L., M. Xie, M. Yang, Y. Yu, S. Zhu, W. Hou, R. Kang, M.T. Lotze, T.R. Billiar, H. Wang, et al. 2014. PKM2 regulates the Warburg effect and promotes HMGB1 release in sepsis. *Nat. Commun.* 5:4436. <https://doi.org/10.1038/ncomms5436>
- Yu, X., and S. Li. 2017. Non-metabolic functions of glycolytic enzymes in tumorigenesis. *Oncogene*. 36:2629–2636. <https://doi.org/10.1038/onc.2016.410>
- Zhang, S., Q. Gao, W. Li, L. Zhu, Q. Shang, S. Feng, J. Jia, Q. Jia, S. Shen, and Z. Su. 2019. Shikonin inhibits cancer cell cycling by targeting Cdc25s. *BMC Cancer*. 19:20. <https://doi.org/10.1186/s12885-018-5220-x>

Supplemental material

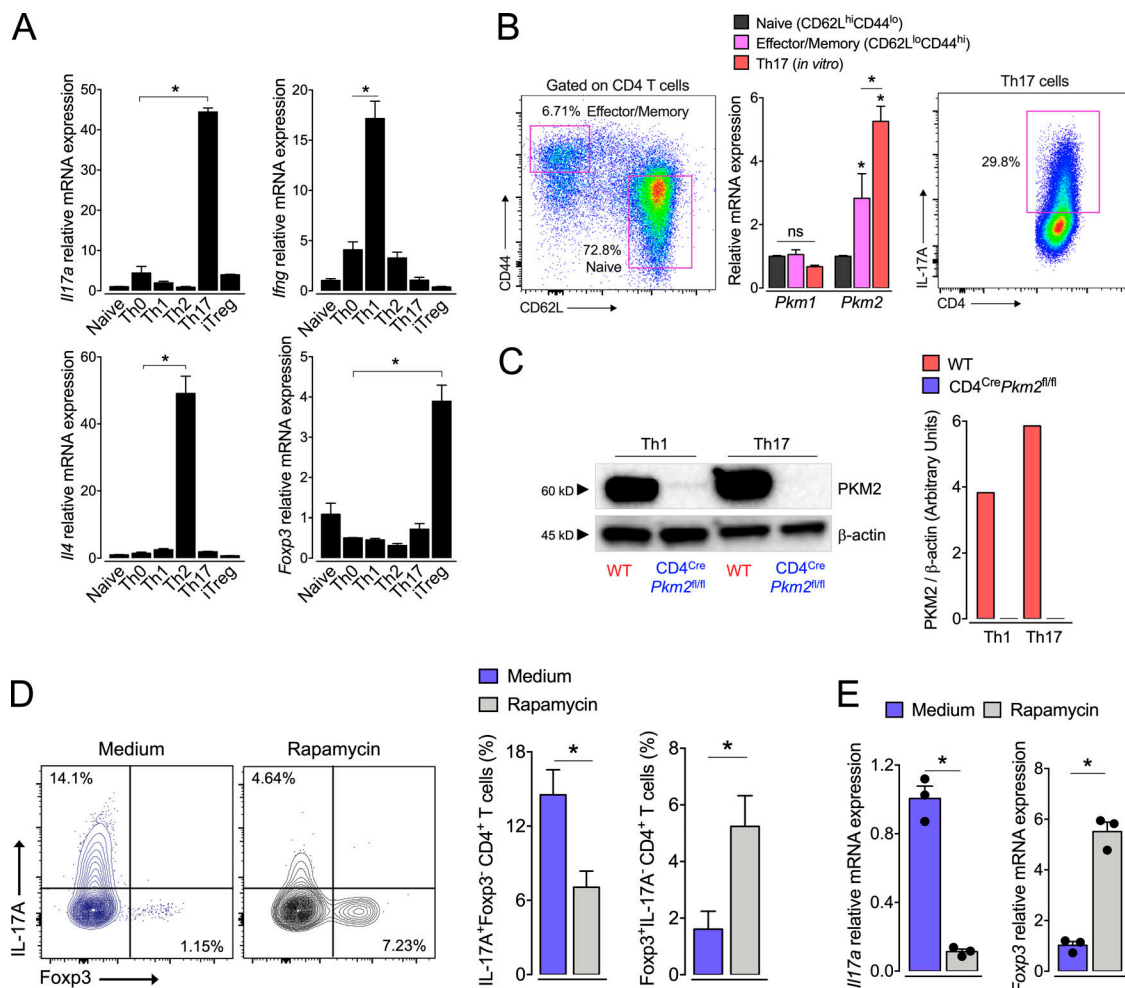


Figure S1. Expression of signature genes of CD4 T cell subsets and differential expression of *Pkm1* and *Pkm2* among naive, effector/memory, and Th17 cells. (A) Naive CD4 T cells were isolated and cultured under Th1, Th2, Th17 or iT reg cells polarizing-conditions; cells were collected, and expression of *Ifng*, *Il4*, *Il17a*, and *foxp3* was determined by RT-qPCR. (B) Naive ($CD4^+CD62L^{hi}CD44^{lo}$) or effector/memory CD4 T cells ($CD4^+CD62L^{lo}CD44^{hi}$) were sorted from LNs and spleen of C57BL/6 WT mice ($n = 3$). Naive cells were also cultured under Th17 cell-polarizing conditions (96 h). Cells were collected, and total mRNA extracted for RT-qPCR analysis. (C) WT or $CD4^{Cre}Pkm2^{fl/fl}$ CD4 T cells were differentiated into Th1 or Th17 cells for 96 h and collected for immunoblot analysis of PKM2 protein expression. β -actin was used as a loading control. (D and E) Rapamycin ($0.1 \mu M$), an mTOR inhibitor, was added to the Th17 cell cultures. Cells were collected and intracellularly stained for IL-17A and Foxp3, followed by flow cytometric analysis; *Il17a* and *Foxp3* gene expression levels were determined by RT-qPCR ($n = 3$). For gene expression analysis, the cycle threshold values were normalized to *Gapdh*; fold change was calculated relative to naive cells (in A and B) or untreated cells (medium; in D and E). Data are representative of two independent experiments. Error bars show mean \pm SEM. P values were determined by two-way ANOVA followed by Tukey's post hoc test (B) or two-tailed Student's *t* test (D and E). *, $P < 0.05$; ns, not significant.

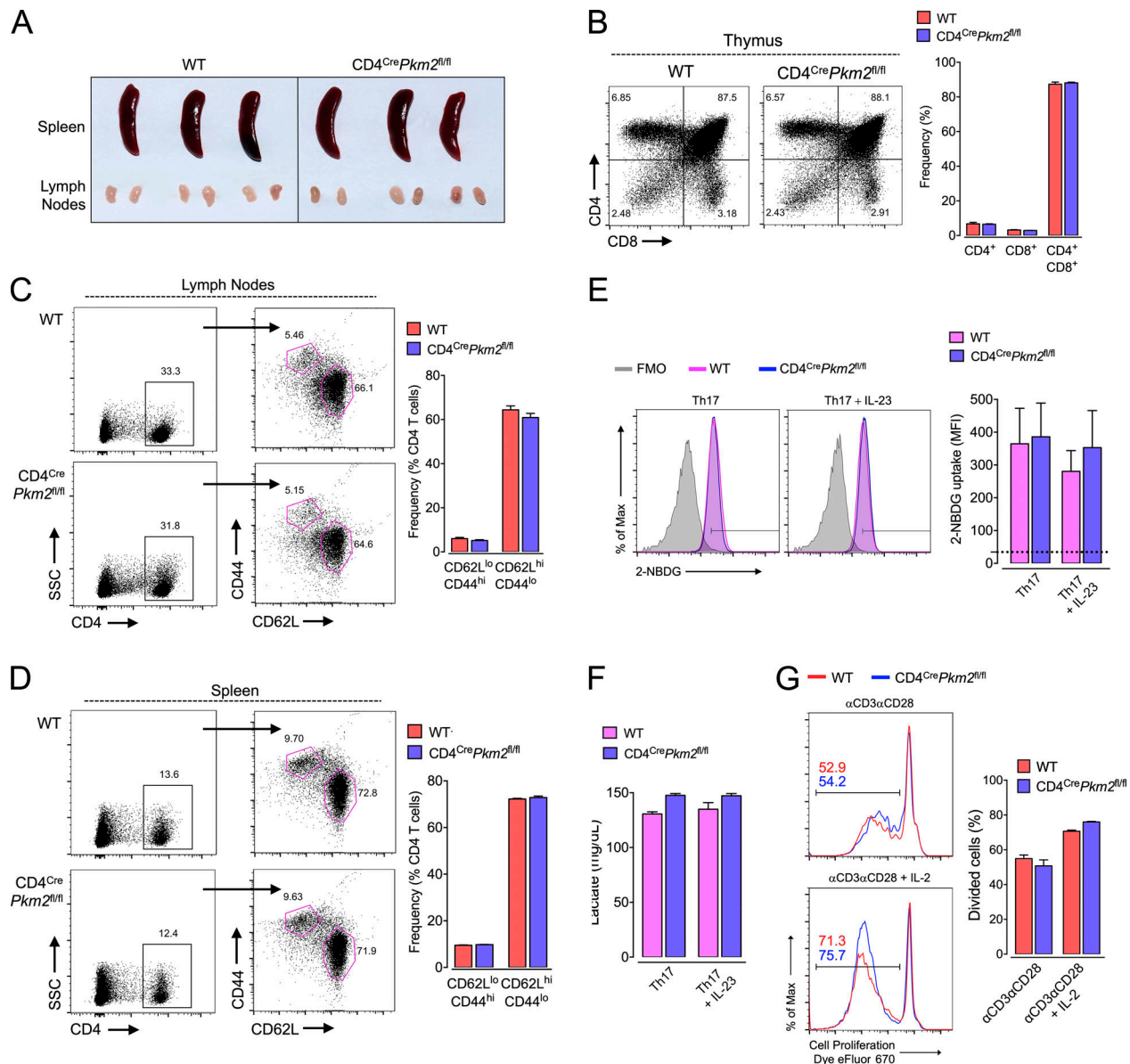


Figure S2. T cell-specific PKM2 deletion in mice does not cause gross defects or affect glucose uptake, lactate production, and proliferation of CD4 T cells. (A) Photograph of spleen and LNs isolated from WT and $CD4^{Cre}Pkm2^{fl/fl}$ mice ($n = 3$). (B) Flow cytometric analyses of thymic $CD4^{+}$ and $CD8^{+}$ frequencies ($n = 3$). (C and D) Proportion of activated ($CD62L^{lo}CD44^{hi}$) and naive ($CD62L^{hi}CD44^{lo}$) CD4 T cells in LNs and spleen ($n = 3$). SSC, side scatter. (E) WT or PKM2-deficient Th17 cells differentiated in the presence or absence of IL-23 were incubated with 2-NBDG (30 μM) for 30 min. The glucose uptake ability of Th17 cells was evaluated by flow cytometry; MFI, mean fluorescence intensity. (F) Levels of lactate produced by Th17 cells were determined in culture supernatants ($n = 3$). (G) Naive CD4 T cells were labeled with 5 μM proliferation dye and then activated with anti-CD3 ϵ /CD28 and cultured in the presence or absence of IL-2 for 72 h. Flow cytometric analyses were performed to determine their proliferative capacity ($n = 3$). Data are representative of two (E and F) or three (B–D) independent experiments. Error bars show mean \pm SEM. P values were determined by two-tailed Student's *t* test.

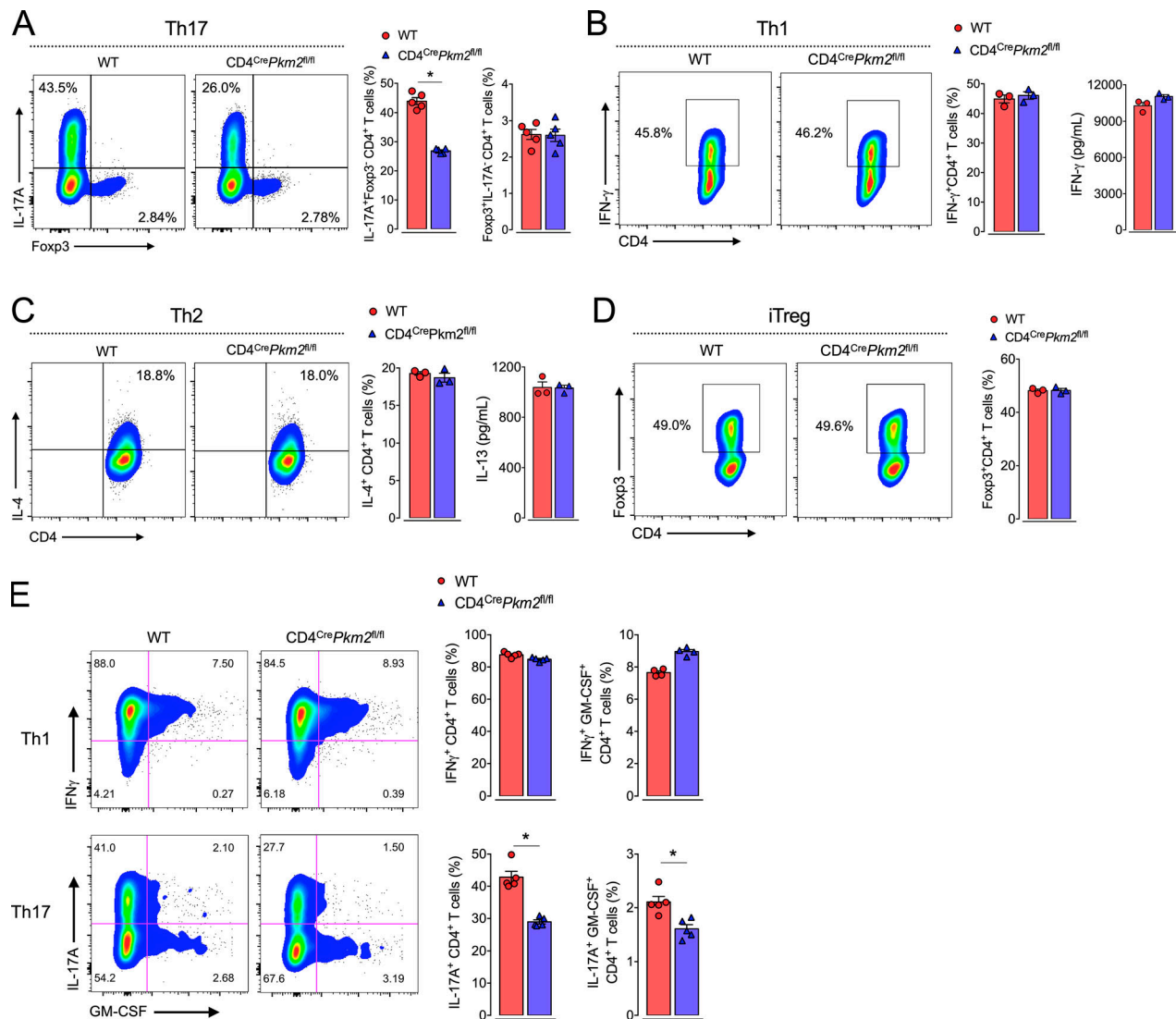


Figure S3. Loss of PKM2 in CD4 T cells does not impair Th1, Th2 or iT reg differentiation. (A) WT or PKM2-deficient CD4 T were cultured under Th17 cell-skewing conditions and stained for both IL-17A and Foxp3, followed by flow cytometric analysis ($n = 5$). (B–D) Naive CD4 T cells were also cultured under Th1, Th2, or iT reg-skewing conditions and analyzed for expression of IFN-γ, IL-4, and Foxp3, respectively, by flow cytometry ($n = 3$). In addition, IFN-γ and IL-13 levels in supernatants of Th1 and Th2 cultures, respectively, were measured by ELISA ($n = 3$). (E) Naive CD4 T cells were cultured under Th1 or Th17 cell-polarizing conditions for 96 h. Intracellular staining for IFN-γ and GM-CSF in Th1 cells (top) and both IL-17A and GM-CSF in Th17 cells (bottom) was performed, followed by flow cytometric analysis ($n = 5$). Data are representative of at least three independent experiments. Error bars show mean \pm SEM. P values were determined by two-tailed Student's t test. *, $P < 0.05$.

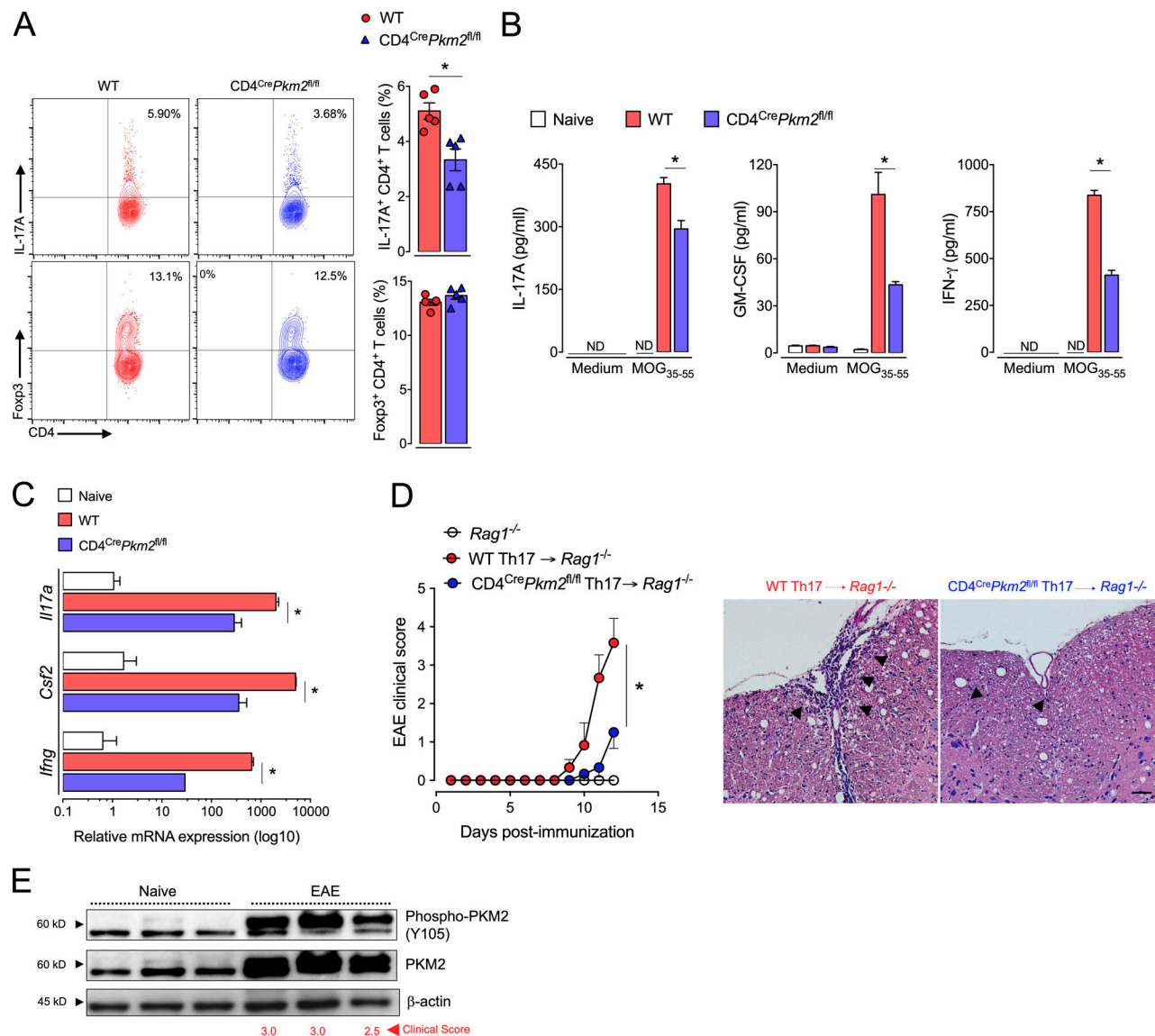


Figure S4. PKM2 boosts Th17 cell-mediated EAE pathogenesis. (A) EAE was induced in WT or CD4^{Cre}Pkm2^{fl/fl} mice and DLN cells collected on day 15 ($n = 5$ per group). Cells were stimulated and intracellularly stained for IL-17A or Foxp3, followed by flow cytometric analysis. (B) DLN cells were harvested and restimulated with MOG₃₅₋₅₅ in vitro for 72 h. The supernatants were collected, and the levels of IL-17A, GM-CSF, and IFN-γ were measured by ELISA ($n = 5$). (C) Lumbar spinal cord sections were collected from naive or EAE mice with PKM2 deficiency in CD4 T cells. Homogenates were obtained and mRNA extracted, followed by cDNA conversion; RT-qPCR was performed to analyze the expression of *Il17a*, *Csf2*, and *Ifng*. *Gapdh* was used for normalization ($n = 5$). (D) DLN cells were collected from WT or CD4^{Cre}Pkm2^{fl/fl} EAE mice (day 8) and cultured in the presence of MOG₃₅₋₅₅ under Th17 cell-skewing conditions for 72 h. CD4 T cells were sorted and intravenously transferred (10^6) into *Rag1*^{-/-} mice. 1 d later, EAE was induced in the recipient mice ($n = 6$ per group). Mice were monitored for clinical signs of EAE and CNS inflammatory cell infiltrate analyzed by H&E staining. Scale bar represents 50 μm. (E) PKM2 and phospho-PKM2 (Y105) protein levels in the spinal cord of EAE-bearing mice were determined by immunoblot. β-actin was used as a loading control. Data are representative of two (A–D) or three (E) independent experiments. Error bars show mean ± SEM. P values were determined by two-way ANOVA followed by Tukey's post hoc test (B–D) and two-tailed Student's *t* test (A). *, $P < 0.05$.

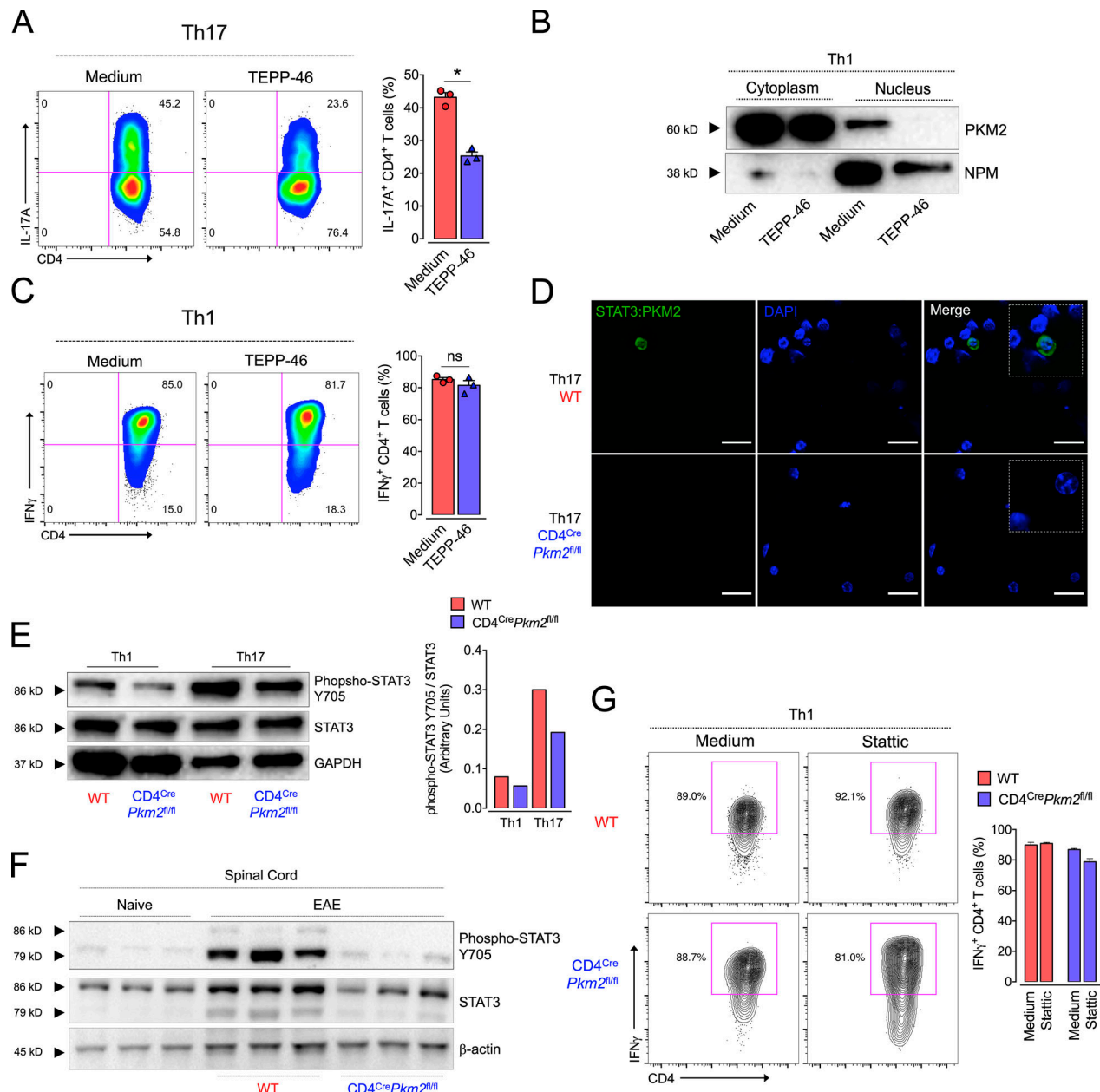


Figure S5. STAT3 activation and PKM2 are dispensable for the generation of Th1 cells. (A) Naive CD4 T cells were cultured under Th17 cell-skewing conditions in the presence or absence of TEPP-46 (100 μM), followed by flow cytometric analysis ($n = 3$). (B and C) Th1 cells were differentiated with or without TEPP-46, and then cytoplasmic and nuclear fractions collected to determine PKM2 protein expression by immunoblot. NPM was used as a nuclear loading control. Flow cytometric analysis of Th1 cell differentiation was conducted ($n = 3$). (D) PLA assay was performed in WT or PKM2-deficient Th17 cells, followed by confocal microscopy analysis. The close proximity of STAT3 and PKM2 is represented in green. The blue signal indicates DAPI-stained nuclei. Scale bar indicates 10 μm. (E) WT or PKM2-deficient Th1 or Th17 cell lysates were subjected to immunoblot analysis of total and phospho-STAT3 (Y705) expression. GAPDH was used as a loading control. (F) STAT3 and phospho-STAT3 (Y705) levels were determined in spinal cords of WT or CD4^{Cre}Pkm2^{fl/fl} EAE-bearing mice by immunoblot analysis. β-Actin was used as a loading control. (G) Naive WT and PKM2-lacking Th1 cells were differentiated in the presence or absence of Stat3 (2 μM); flow cytometric analysis of IFN-γ-producing cells was performed ($n = 3$). Data are representative of two (B–G) or three (A) independent experiments. Error bars show mean ± SEM. P values were determined by two-way ANOVA followed by Tukey's post hoc test (G) and two-tailed Student's *t* test (A and C). *, $P < 0.05$; ns, not significant.

Tables S1 and S2 are provided online as separate Word documents. Table S1 lists mouse primer pairs used for RT-qPCR analysis. Table S2 lists reagents used in this study.